NAVAL POSTGRADUATE SCHOOL
Monterey, California

THESIS

A NUMERICAL SIMULATION OF SEASONAL CIRCULATION IN THE SOUTH CHINA SEA

by

Ching-Chung Li

March 1994

Thesis Advisor: Peter C. Chu

Thesis Co-advisor: Dong S. Ko

Approved for public release; distribution is unlimited.

REPORT DOCUMENTATION PAGE

Form Approved
OMB No. 0704-0188

1. AGENCY USE ONLY *(Leave blank)*	2. REPORT DATE	3. REPORT TYPE AND DATES COVERED
	March 1994	Master's Thesis

4. TITLE AND SUBTITLE
A NUMERICAL SIMULATION OF SEASONAL CIRCULATION IN THE SOUTH CHINA SEA

5. FUNDING NUMBERS

6. AUTHOR(S)
Ching-Chung Li

7. PERFORMING ORGANIZATION NAME(S) AND ADDRESS(ES)
Naval Postgraduate School

Monterey, CA 93943-5000

8. PERFORMING ORGANIZATION REPORT NUMBER

9. SPONSORING/MONITORING AGENCY NAME(S) AND ADDRESS(ES)

10. SPONSORING/MONITORING AGENCY REPORT NUMBER

11. SUPPLEMENTARY NOTE
The views expressed in this thesis are those of the author and do not reflect the official policy or position of the Department of Defense or the United States Government.

12a. DISTRIBUTION/AVAILABILITY STATEMENT
Approved for public release;

Distribution is unlimited.

12b. DISTRIBUTION CODE

13. ABSTRACT *(Maximum 200 words)*

The circulation in the South China Sea (SCS) is mainly determined by the monsoons. This monsoon-induced circulation is connected with the circulation in the Pacific Ocean to a small extent and linked with that of the Indian Ocean only by the Timor Current. During winter, the water enters the South China Sea at the north through Formosa Strait and Luzon Strait, and exits at the south through Karimata Strait. During summer, the circulation reverses, the water enters at the south and exits at the north. Water from the north is generally cooler than water from the south. The northward (southward) flow induces warm (cold) advection. Therefore, the seasonal cycle of the circulation in the South China Sea becomes a major factor controlling the seasonal cycle of the sea surface temperature, which might effect the seasonal variation of the Eastern Asian monsoon system. In the preliminary results, the seasonal circulation and temperature patterns simulated by the primitive equation model are similar to those reported by Wyrtki(1961). Yet, our model is better than the Pohlmann (1987) shallow-water model and shows more details.

14. SUBJECT TERMS	15. NUMBER OF PAGES
Open Boundary, Turbulence Closure, Temperature, Salinity, Circulation Monsoons	85
	16. PRICE CODE

17. SECURITY CLASSIFICATION OF REPORT	18. SECURITY CLASSIFICATION OF THIS PAGE	19. SECURITY CLASSIFICATION OF ABSTRACT	20. LIMITATION OF ABSTRACT
UNCLASSIFIED	UNCLASSIFIED	UNCLASSIFIED	UL

NSN 7540-01-280-5500

Standard Form 298 (Rev. 2-89)
Prescribed by ANSI Std. Z39-18

Approved for public release; distribution is unlimited

A NUMERICAL SIMULATION OF SEASONAL CIRCULATION IN THE SOUTH CHINA SEA

by
Ching-Chung Li
Lieutenant, Republic of China Navy
B.S., Chung Cheng Institute of Technology, 1987

Submitted in partial fulfillment of the
requirements for the degree of

MASTER OF SCIENCE IN PHYSICAL OCEANOGRAPHY

from the

NAVAL POSTGRADUATE SCHOOL
March 1994

Author: Ching-Chung Li

Ching-Chung Li

Approved By: Peter Cheng Chu

Peter C. Chu, Thesis Advisor

DongShan Ko

Dong S. Ko, Thesis Co-advisor
RSMAS, University of Miami

Robert H. Bourke for

Curtis A. Collins, Chairman,
Department of Oceanography

ABSTRACT

The circulation in the South China Sea (SCS) is mainly determined by the monsoons. This monsoon-induced circulation is connected with the circulation in the Pacific Ocean to a small extent and linked with that of the Indian Ocean only by the Timor Current. During winter, the water enters the South China Sea at the north through Formosa Strait and Luzon Strait, and exits at the south through Karimata Strait. During summer, the circulation reverses, the water enters at the south and exits at the north. Water from the north is generally cooler than water from the south. The northward (southward) flow induces warm (cold) advection. Therefore, the seasonal cycle of the circulation in the south China Sea becomes a major factor controlling the seasonal cycle of the sea surface temperature, which might effect the seasonal variation of the Eastern Asian monsoon system.

In the preliminary results, the seasonal circulation and temperature patterns simulated by the primitive equation model are similar to those reported by Wyrtki (1961). Yet, our model is better than the Pohlmann (1987) shallow-water model and shows more details.

TABLE OF CONTENTS

I. INTRODUCTION 1

II. BACKGROUND 11

A. CONFIGURATION OF THE SOUTH CHINA SEA 11

B. ATMOSPHERIC FORCING 16

1. Low-Level Atmospheric Circulation 16

2. Buoyancy Flux at Air-Sea Interface 16

C. OCEANIC CIRCULATIONS 20

1. The Equatorial Current System 20

2. The Kuroshio Intrusion Through the Luzon Strait 21

3. The Formosa Strait 23

4. The Java Sea 23

5. The Strait of Malacca 25

6. The Gulf of Thailand 25

7. The South China Sea 25

D. WATER MASSES 27

1. Mass Transport 27

2. Temperature and Salinity 30

III. NUMERICAL MODEL 36

A. INTRODUCTION 36

B. MODEL FEATURES 38

C. MODEL GOVERNING EQUATIONS 38

1. The Continuity Equation 39

2. The Renolds Momentum Equations 39

3. The Conservation Equations for Temperature and Salinity 39

D. TURBULENCE CLOSURE 40
E. SURFACE AND BOTTOM BOUNDARY CONDITIONS 41
F. σ COORDINATE SYSTEM 42
G. INITIAL CONDITIONS 43
H. OPEN BOUNDARY CONDITIONS 43
I. ATMOSPHERIC FORCING 44
IV. MODEL RESULTS 49
A. SURFACE CIRCULATION 50
1. PSCS Model Results 50
2. Comparisons 53
B. TEMPERATURE AND SALINITY 60
1. PSCS Model Results 60
2. Comparisons 66
a. Temperature 66
b. Salinity 67
V. CONCLUSIONS 68
LIST OF REFERENCES 71
INITIAL DISTRIBUTION LIST 74

LIST OF TABLES

TABLE 1: THE STRAITS CONNECTING THE SOUTH CHINA SEA WITH ADJACENT SEAS 11

TABLE 2: THE ANNUAL TOTAL PRECIPITATION AND HEATING PROPERTIES OF THE SOUTHEAST ASIAN WATERS (Wyrtki, 1961) 19

TABLE 3: MASS TRANSPORT (Sv) OF CUASIAN WATERS (Wyrtki, 1961) 30

TABLE 4: MONTHLY MASS TRANSPORT (Sv) AT THE OPEN BOUNDARIES 43

TABLE 5: COMPARISON BETWEEN THE NAGA REPORT AND MODELING RESULTS (SUMMER) 56

TABLE 6: COMPARISON BETWEEN THE NAGA REPORT AND MODELING RESULTS(WINTER) 57

TABLE 7: COMPARISON OF CURRENT SPEED BETWEEN THE NR OBSERVATIONS AND THE PSCS MODEL RESULTS (JUNE) 59

TABLE 8: COMPARISON OF CURRENT SPEED BETWEEN THE NR OBSERVATIONS AND THE PSCS MODEL RESULTS (DECEMBER) 59

LIST OF FIGURES

Figure 1: Location of the South China Sea 2

Figure 2: The Bottom Topography of the South China Sea (Depth Contours in Meters) 3

Figure 3A: Observational Summer (June) Surface Circulation of the Southeast Asian Waters (Wyrtki, 1961) 4

Figure 3B: Observational Winter (December) Surface Circulation of the Southeast Asian Waters (Wyrtki, 1961) 5

Figure 4A: Shallow Water Model Simulating the Summer Surface Circulation of the South China Sea (Pohlmann, 1987) 7

Figure 4B: Shallow Water Model Simulating the Winter Surface Circulation of the South China Sea (Pohlmann, 1987) 8

Figure 5A: The Bottom Topography of the Gulf of Thailand (Wyrtki, 1961) 14

Figure 5B: The Bottom Topography of the Luzon Strait (Shaw, 1989) 15

Figure 6: The Mean 850-mb Streamline of the Southeast Asia Monsoons (a) December, (b) July (Cheang, 1987) 17

Figure 7: Average Rainfall (mm/yr) of the Southeast Asian Waters, Higher than 4000 mm Dashed (Wyrtki, 1961) 18

Figure 8: The Deep Water Connections Between the Pacific and Indian Oceans (Broecker et al., 1986) 22

Figure 9: Seasonal Variation of the Current System Near the Luzon Strait (Huang, 1988) 24

Figure 10A: Summer (June) Mass Transport (Sv) of the Southeast Asian Waters (Wyrtki, 1961) 28

Figure 10B: Winter (December) Mass Transport (Sv) of the Southeast Asian Waters (Wyrtki, 1961) 29

Figure 11A: Levitus Surface Temperature Distribution (June); Interval = 1°C 31

Figure 11B: Levitus Surface Temperature Distribution (December); Interval = 1°C 32

Figure 12A: Levitus Surface Salinity Distribution (June); Interval = 0.25 psu 33

Figure 12B: Levitus Surface Salinity Distribution (December); Interval = 0.25 psu 34

Figure 13: Model Grid 37

Figure 14A: Summer (May) Hellerman Wind Stress Distribution 45

Figure 14B: Summer (June) Hellerman Wind Stress Distribution 46

Figure 14C: Winter (November) Hellerman Wind Stress Distribution 47

Figure 14D: Winter (December) Hellerman Wind Stress Distribution 48

Figure 15A: Simulated Summer (10 May) Surface Circulation 51

Figure 15B: Simulated Summer (30 June) Surface Circulation 52

Figure 15C: Simulated Winter (5 November) Surface Circulation 54

Figure 15D: Simulated Winter (10 December) Surface Circulation 55

Figure 16A: Simulated Summer (30 June) Surface Temperature(°C) Distribution; Interval = 1°C 61

Figure 16B: Simulated Winter (10 December) Surface Temperature (°C) Distribution; Interval = 1°C 62

Figure 17A: Simulated Summer (30 June) Surface Salinity (psu) Distribution; Interval = 0.25 psu 63

Figure 17B: Simulated Winter (10 December) Surface Salinity (psu) Distribution; Interval = 0.25 psu 64

ACKNOWLEDGEMENT

I would like to express my sincere appreciation to my advisor, Professor Peter C. Chu, for his inspiration and guidance throughout the course of my thesis research at the Naval Postgraduate School. I would also like to thank my co-advisor, Dr. Dong-San Ko, for his invaluable help in the technical aspects of completing this thesis. I dedicate this work to Mrs. Ko, my wife, Whey-Ming, and my children, Kai-lin and Sean, for their moral support and understanding over the duration of this research.

I. INTRODUCTION

The South China Sea, with the Gulf of Thailand included, is the largest marginal sea of the Southeast Asian Waters (Figure 1). It is separated from adjacent oceans by the chain of the Southeast Asian Islands and contains the broad shallow Sunda Shelf on the south, a shelf extending from the Gulf of Tonkin to Formosa Strait on the north, a deep sea basin in the center, and the Dangerous Ground with numerous reef islands over the southeast (Figure 2). From 1959 to 1961 a Naga expedition was carried out by the Sripps Institution of Oceanography of University of California and jointly sponsored by the governments of the former South Vietnam, Thailand, and the United States of America. It provided the observational results of marine investigations of the South China Sea (Wyrtki, 1961).

In summer (June), the southwest monsoon prevails and surface currents flow northeastward entering the South China Sea through the Gasper and Karimata Straits (Figure 3A). The largest part of the South China Sea water masses pass south of Taiwan into the root of the Kuroshio Current; a small part flows northwards through the Formosa Strait joining the Kuroshio Current. A current develops off the coast of Borneo towards the southwest with a current speed between 0.12 m/s and 0.25 m/s, which turns back to the north in the region of Natuna Island. Along the coast of Luzon, water flows northwards from the Sulu Sea with a surface current speed between 0.12 m/s and 0.25 m/s. A jet current flows from Vietnam to the Luzon Strait with a current speed of 0.25 m/s to 0.30 m/s.

In winter (December), the northeast monsoon prevails and surface currents flow southwestward entering the South China Sea through the Formosa and Luzon Straits (Figure 3B). Waters from the Kuroshio Current and the East China Sea enter the South China Sea flowing southwestward along the coastline of Asia and flow out of the South China Sea through the Gasper and Karimata Straits. The surface current speeds are about

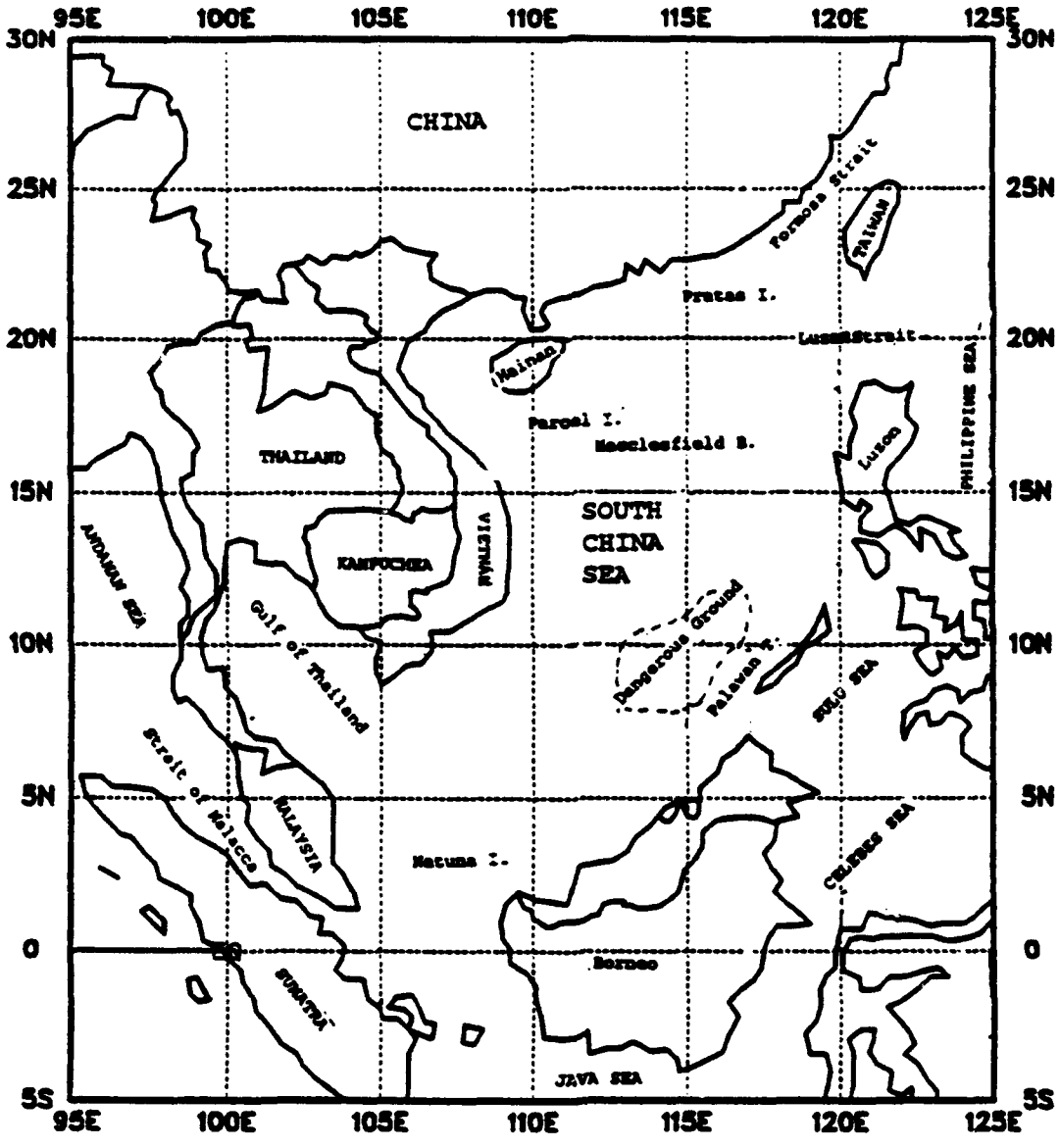

Figure 1 : Location of the South China Sea

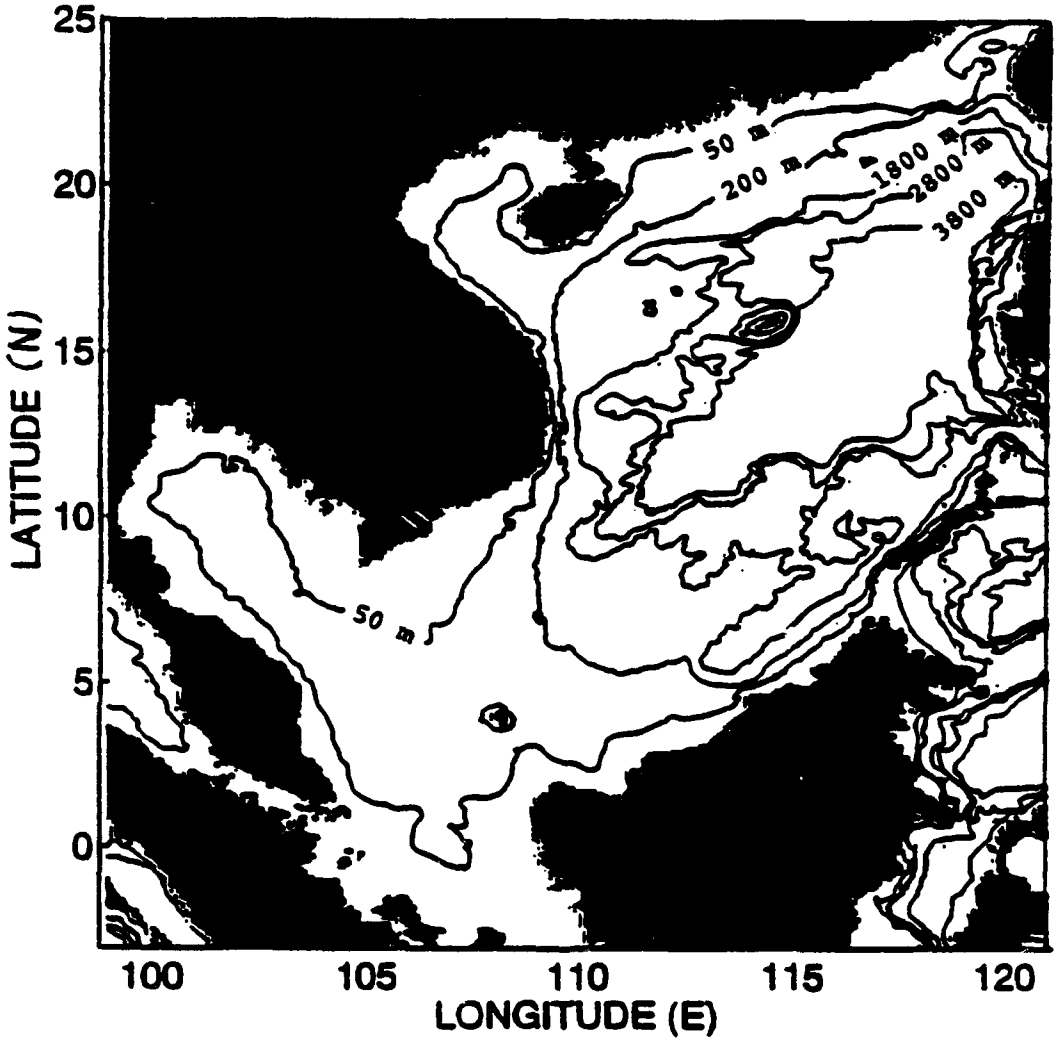

Figure 2 : The Bottom Topography of the South China Sea (Depth Contours in Meters)

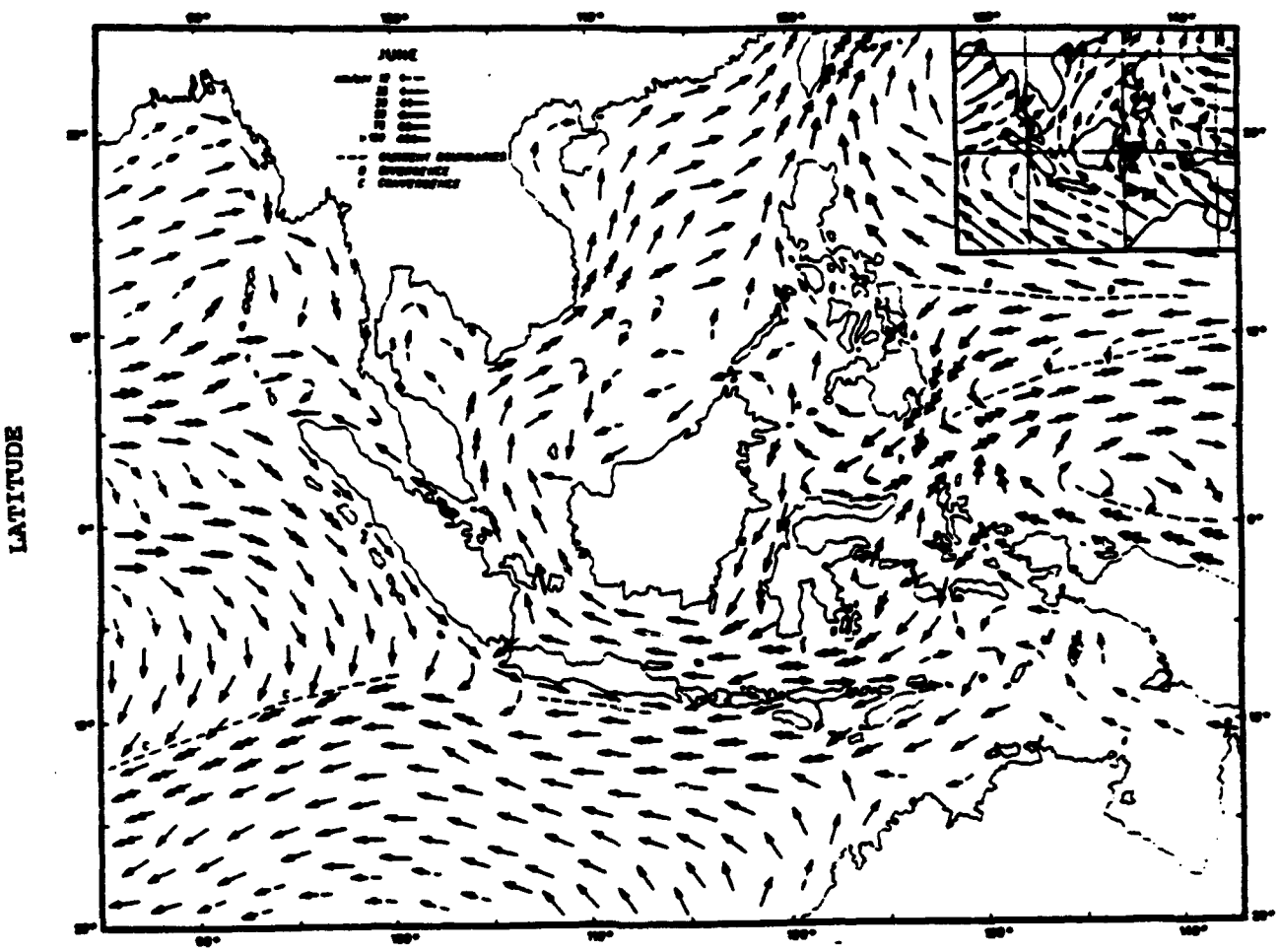

Figure 3A : Observational Summer (June) Surface Circulation of the Southeast Asian Waters (Wyrtki, 1961)

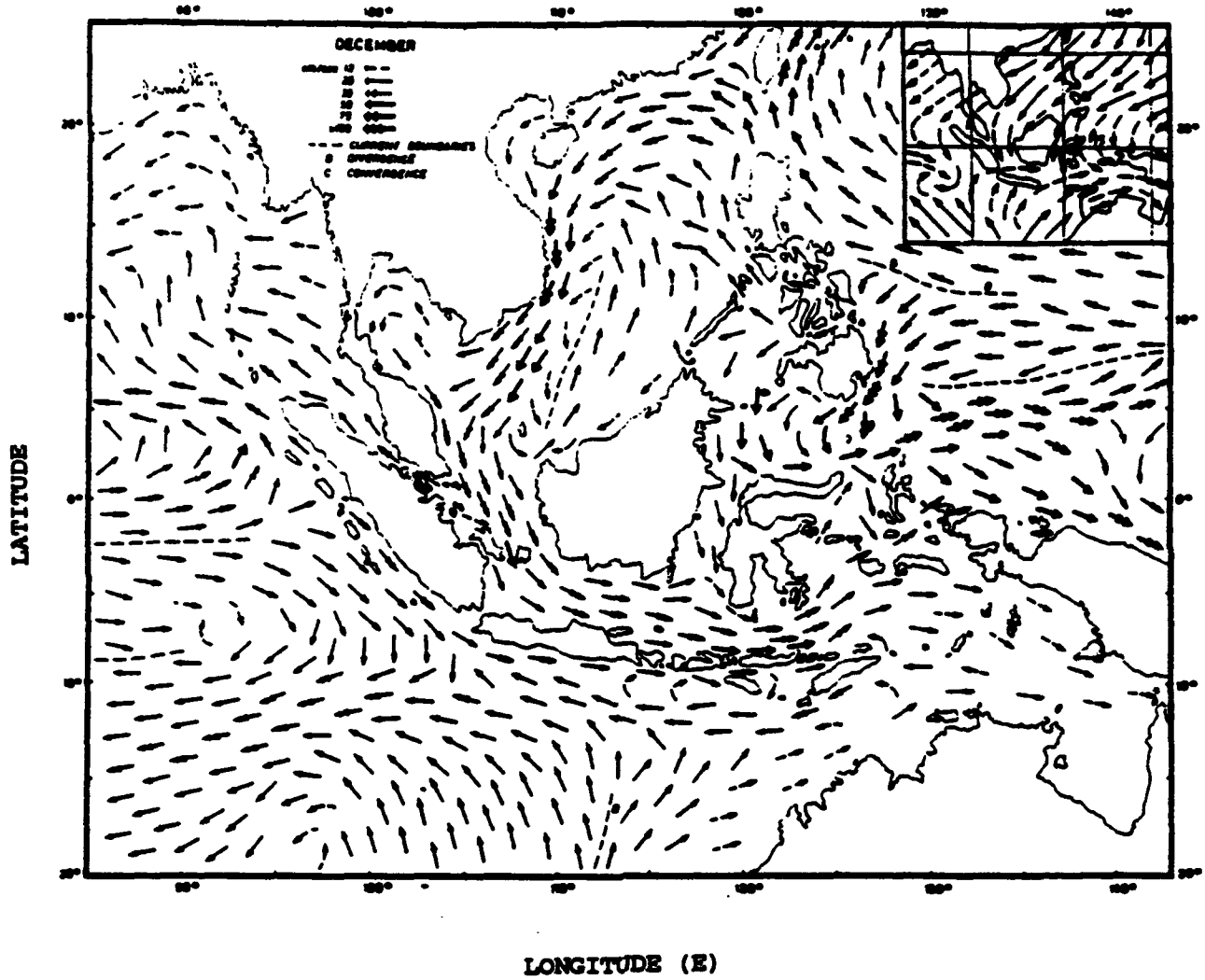

Figure 3B : Observational Winter (December) Surface Circulation of the Southeast Asian Waters (Wyrtki, 1961)

0.5 m/s off the Hainan coast, about 0.75 m/s off the coast of Vietnam, and about 0.3 m/s in the Gasper Strait. The counter current in the center of the South China Sea is present and lies farther to the east because of the strength of the main current. From the Sulu Sea water flows into the South China Sea and is mixed into the main current. A current boundary exists between Vietnam and Borneo and a very weak (less than 0.12 m/s) southwestward flow occurs along the coast of Borneo which encounter the waters from the north flowing northward along the right hand side of the current boundary.

Pohlmann (1987) used a 12-layer shallow water circulation model to study the responses of the South China Sea to the east Asian monsoons. The model horizontal grid size is about 50 km. The simulated mean surface circulation for the summer and winter seasons is shown in Figures 4A and 4B, respectively. Since they do not show the current speed clearly, we only describe the surface circulation patterns as follows.

In summer, waters from the Java Sea enter the South China Sea through the Gasper and Karimata Straits flowing clockwise and eastward from the southern coast of Vietnam to Borneo. Then, it flows northward along the coast of Palawan and Luzon to west of the Luzon Strait. In the northern South China Sea, there is a cyclonic circulation between Hainan and the Luzon Strait. A small amount of Kuroshio current flows into the South China Sea and meets the waters from Borneo flowing westward, and then it encounters the cyclonic circulation flowing northward out of the South China Sea through the Formosa Strait. In winter, waters from the Philippine Sea enter the northern South China Sea through the Luzon Strait. A small amount of water flows northward, through the Formosa Strait, out of the South China Sea. Most parts of it flow westward and cyclonically from the Luzon Strait to Hainan and then it flows southward along the coast of Vietnam toward Singapore. It then flows eastward entering the Java Sea through the Gasper and Karimata Straits. There is another branch of water flowing southward along the coastlines of Luzon, Palawan, and Boreno to Natuna Island. On its way from Luzon to Natuna Island, waters continuously separate and flow westward spreading all over the central South China Sea toward the Asian coastline.

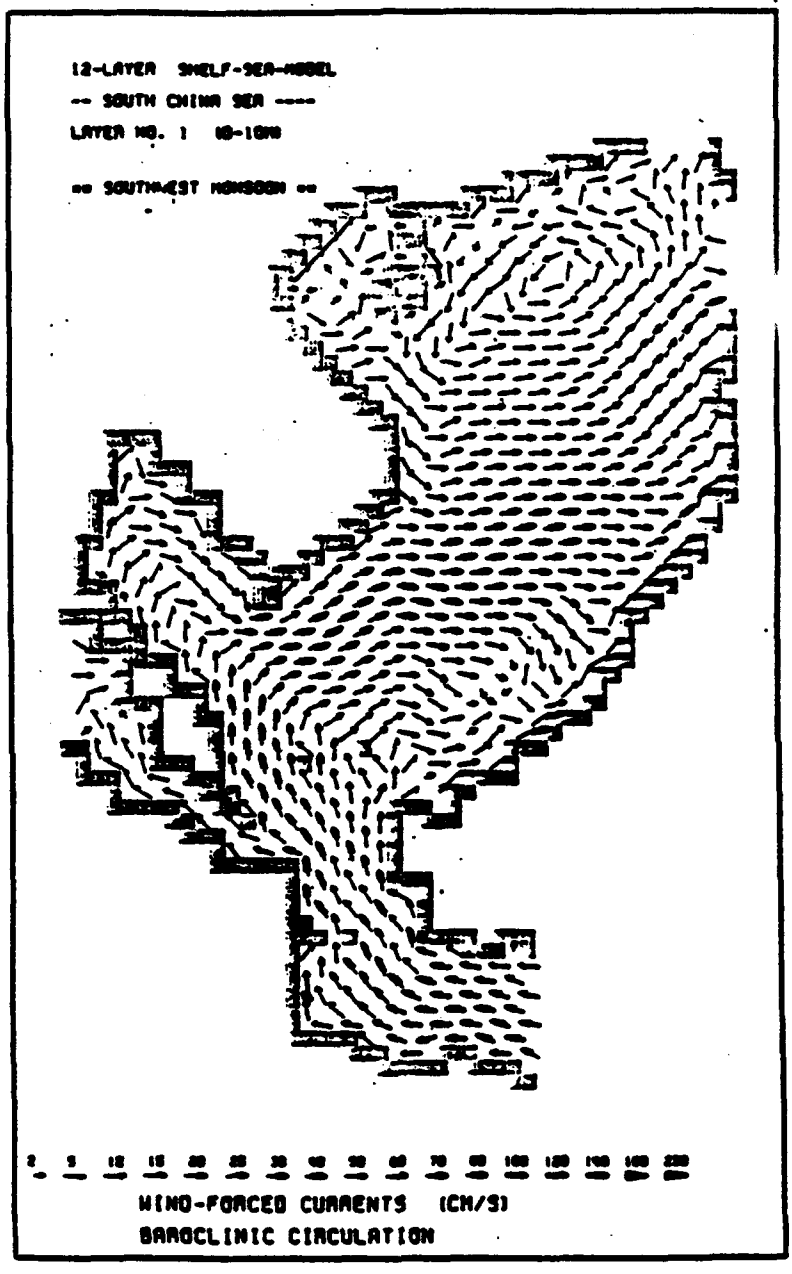

Figure 4A : Shallow Water Model Simulating the Summer Surface Circulation of the South China Sea (Pohlmann, 1987)

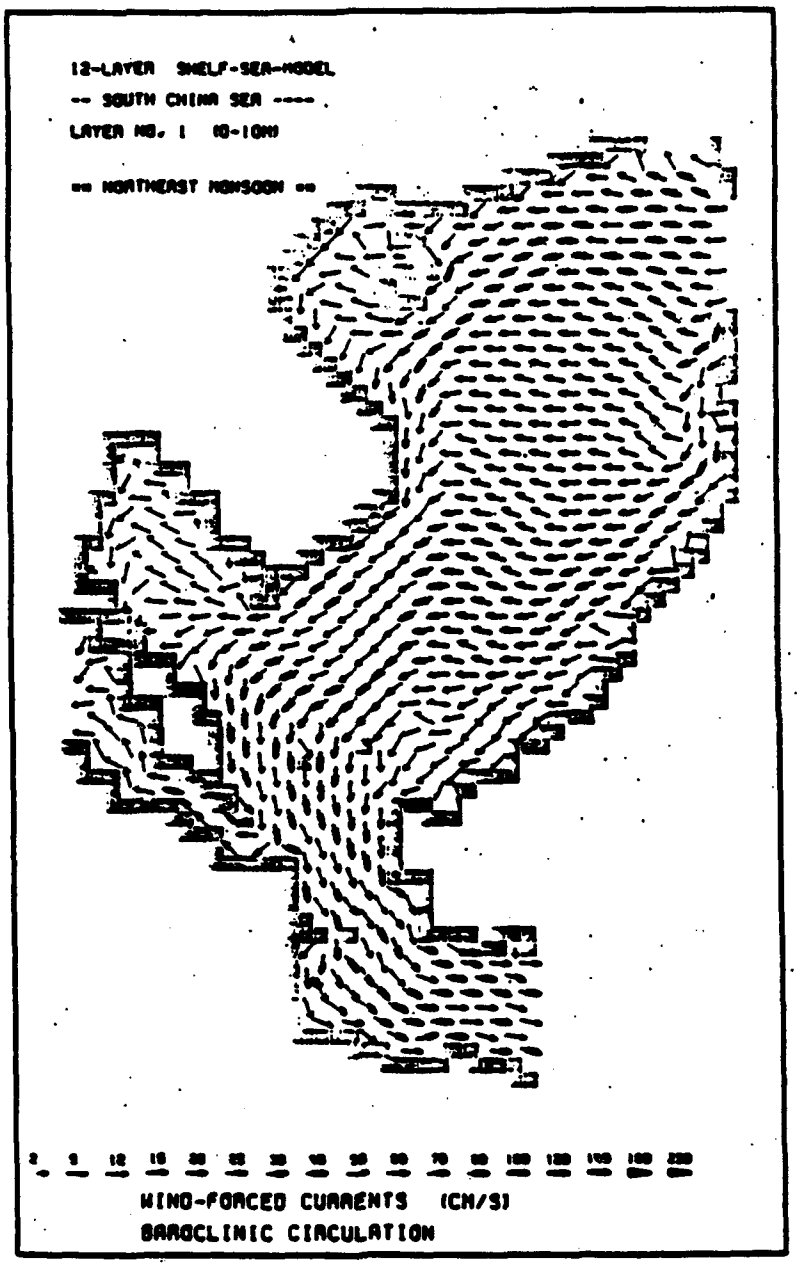

Figure 4B : Shallow Water Model Simulating the Winter Surface Circulation of the South China Sea (Pohlmann, 1987)

This model predicts the seasonal varying surface currents quite reasonable when compared with the Wyrtki (1961) atlas. The currents are generally northward during winter and change to southward during summer. However, there is no jet branching during summer, and the model simulated current pattern in the central South China Sea is different from the Naga Report observations (Figure 3A). Moreover, during winter the model simulated currents at the Luzon western coast, Formosa Strait, and the Dangerous Ground (Spratly Islands) are oppositely directed compared with the observations summarized in the Naga Report (Figure 3B). As pointed out by Pohlmann, the shallow water model might not be appropriate for the South China Sea due to the complex topography.

A three-dimensional, primitive equation ocean circulation model with free surface developed at Princeton University (Blumberg and Mellor, 1987) will be used to study the South China Sea response to the monsoon system. The principle attributes of this model are as follows.

*It contains an imbedded second moment turbulence closure sub-model (Mellor and Yamada, 1982) to provide vertical mixing coefficients.

*It is a sigma coordinate model in that the vertical coordinate is scaled on the water column depth.

*The horizontal grid uses curvilinear orthogonal coordinates and an "Arakawa C" differencing scheme.

*The horizontal differencing is explicit whereas the vertical differencing is implicit. The latter eliminates time constraints for the vertical coordinate and permits the use of fine vertical resolution in the surface and bottom boundary layers.

*The model has a free surface and a split time step. The external mode portion of the model is two-dimensional and uses a short time step (25 sec) based on the Courant-Friedrichs-Levy (CFL) computational stability condition and the external wave speed. The internal mode is three-dimensional and uses a long time step (900 sec) based on the CFL condition and the internal wave speed.

*Complete thermodynamics have been implemented.

The grid size of this 23-level model is about 20 km in the horizontal. It will deal with both the shelf sea and the deep ocean regions in the modeling process and provide the numerical results to help us understand the dynamics of the South China Sea. The observations from the Naga Report are used for determining the open boundary conditions and for verifying the model results. The Levitus data set is used for initializing the model and for verifyirg the model results.

The structure of this thesis is described as follows. Chapter II describes the background of the South China Sea which is based on the Naga Report and other supplements. Chapter III introduces the numerical model and the data sources used in this study. Chapter IV presents the model simulated results. Chapter V is the conclusions and the future recommendations.

II. BACKGROUND

A. CONFIGURATION OF THE SOUTH CHINA SEA

The South China Sea is situated between the Pacific and Indian Oceans and formed by the Asian coastline and the chain of marginal islands of the Southeast Asian Waters. It extends about 3380 km from Taiwan to Singapore and about 1690 km from Hainan to Palawan. Table 1 shows the straits connecting the South China Sea with adjacent seas. It consists of many particular geographical features such as a deep sea basin, an ocean plateau, and a continental shelf, and these features make its regional bottom topography and oceanic appearances complex (Figure 2).

TABLE 1: THE SRAITS CONNECTING THE SOUTH CHINA SEA WITH ADJACENT SEAS

Adjacent Seas	Straits	Sill Depth(m)	Ocean System
East China Sea	Formosa Strait	70	Pacific
Philippine Sea	Luzon Strait	2600	Pacific
Sulu Sea	Mindoro Strait	450	Pacific
Sulu Sea	Balabac Strait	100	Pacific
Java Sea	Karimata Strait	<40	Pacific
Java Sea	Gasper Strait	<40	Pacific
Java Sea	Banka Strait	closed at southern end	Pacific
Andaman Sea	Strait of Malacca	100(west),30(east)	Indian

Its northern part is a continental shelf which includes the Gulf of Tonkin, Formosa Strait, Hainan, and Taiwan. The average widths of this shelf are 152 km along mainland

China and 10 km from most southern point of Taiwan. The Gulf of Tonkin deepens from the coast gradually to the center with a maximum depth of 70 m. On the other hand, the Formosa Strait is about 150 km wide, 60 m deep in the northern part and 50 m deep in the southern part (Gilg, 1970).

The west and north central shelf areas are part of a submerged Asian continental margin which extend southward from the south of Formosa Strait and eastward from the coast of Vietnam into the central basin, respectively. It consists of a continental slope, numerous coral reefs and several ocean valleys. In the north central part there are numerous peaks of reef such as: Pratas Reefs, Helen Shoal, Paracel Island and Reefs, and Macclesfield Bank. The terrace east of Pratas lies between 2400 and 2950 m and is exceptionally deep. Most of the coral reefs occur on or within the terraces; however, Macclesfield Bank is an exceptionally large reef which is not related to a terrace. This bank and several large ridges to the south do not reach sea level and appear to extend with a steep slope to the basin floor on the east (Gilg, 1970).

The central part is a deep sea central basin with a maximum depth more than 4300 m. The south central part is a plateau with reefs called the Spratly Islands or the Dangerous Ground. There are numerous reefs and islands on this plateau and they generally lie in 1470 to 2010 m depth. Only the Reed Bank in the northeast is shallower and its base appears to lie in 300 to 500 m depth (Wyrtki, 1961). There is a channel with a sill depth about 2050 m through the reef region connecting the central basin and Palawan Trough. However, the Palawan Trough appears to connect with the central basin by way of a valley with a sill depth about 1400 m on the northeast side of Reed Bank, too. Moreover, an apron of sediments is present at the south end of the Dangerous Ground and coral reefs appear less numerous here (Gilg, 1970).

The Gulf of Thailand is situated on the western side of the Sunda Shelf and its mouth opens about 338 km wide into the South China Sea. The distance from the head of the Gulf to its mouth is about 760 km with its greatest width about 500 km. Its bottom topography is shown in Figure 5A and its deepest place is about 80 m deep at the central part of Gulf.

The northeastern coast is generally shallower and flatter than the southwestern coast. The deeper central gulf is separated from the South China Sea by two ridges. One of them extends southwestward at depths of less than 25 m for more than 100 km from Cape Camau. The other deeper ridge extends northeastward off Kota Bharu for a distance of 152 km at depths less than 50 m. In the narrow deeper channel between the ridges a sill depth of 67 m was observed (Wyrtki, 1961).

On the eastern side is a submerged island margin with the deep Palawan Trough of more than 3400 m depth. The slope of this margin is very steep near Palawan and Luzon. The average shelf widths of this margin are 10 km from Luzon, 50 km from Palawan, and 84 km off Borneo (Gilg, 1970). It connects the Sulu Sea and the Pacific Ocean with the Balabac, Mindoro Straits and Luzon Strait, respectively. In the Luzon Strait, which is between Taiwan and Luzon, there is a depression in the form of a deep channel that extends northeastward across the submarine ridge called Bashi Channel (Figure 5B). This channel is 3100 to 3600 m deep throughout its length, except for sills of 1830 and 2380 m off the tip of Taiwan. Numerous small channels and valleys connect this deep channel with the Pacific Basin across the submarine ridge north of Luzon. One of them, northwest of Y'Ami Island, has a sill depth of 2600 m and is probably the passage of main water interchange between the South China Sea and the Pacific Ocean. The other channels across this ridge have sill depths of 730 to 1300 m (Gilg, 1970).

The southern part of the South China Sea is the Sunda Shelf which is situated between Malaysia, Sumatra, Java, and Borneo. It connects the Andaman Sea through the Strait of Malacca and connects the Java Sea through Karimata Strait and Gasper Strait, respectively. It is a very flat shallow trough with depths between 40 to 100 m at its central part and depths which decrease south of the equator to less than 40 m. However, there are several submerged river valleys which lie on the bottom of the Sunda Shelf between Borneo, Sumatra, and Singapore. They drain the land and join together flowing northward into the south central plateau area. These movements transport the riverine sediments and gradually

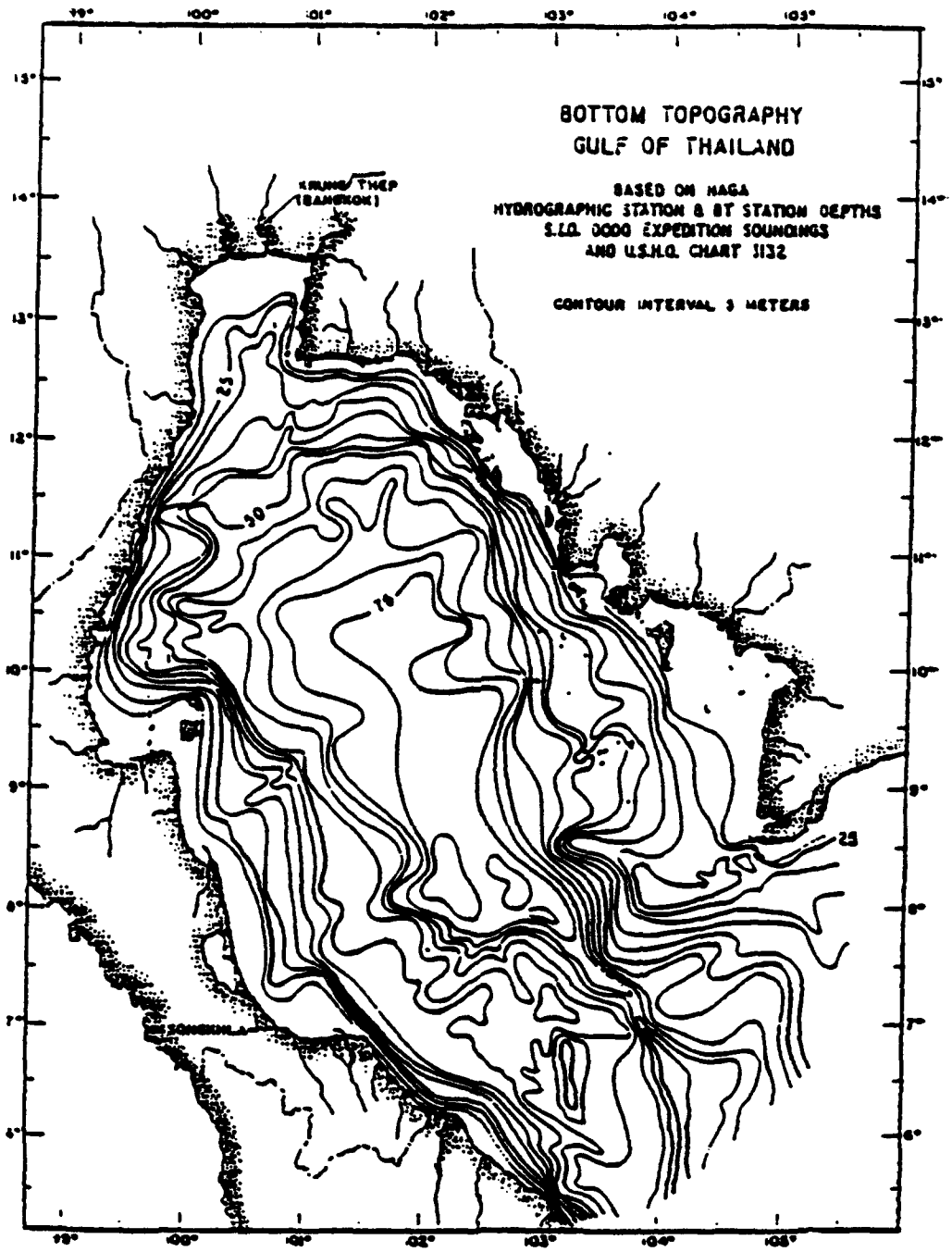

Figure 5A : The Bottom Topography of the Gulf of Thailand (Wyrtki, 1961)

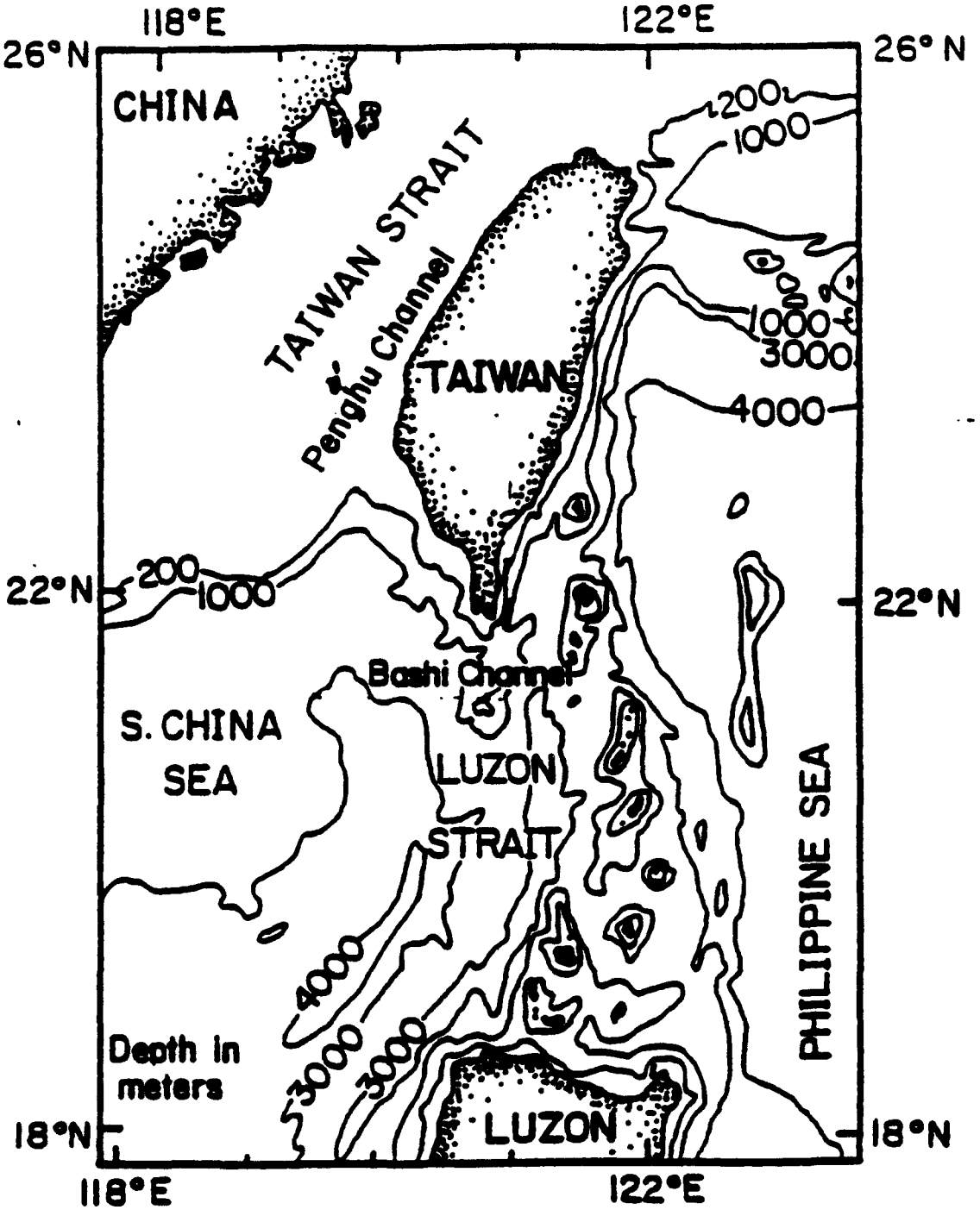

Figure 5B : The Bottom Topography of the Luzon Strait (Shaw, 1989)

make the water depth shallower in the southern part of the Sunda Shelf. Similar features are also found in the Gulf of Thailand (Wyrtki, 1961).

B. ATMOSPHERIC FORCING

1. Low-Level Atmospheric Circulation

The South China Sea is an ideal region for monsoon development. Hess (1959) pointed out that the monsoon changes with season over Asia as a direct and simple response to the low continental temperatures in winter and the high continental temperatures in summer. Figure 6 shows the mean December and July 850-mb streamline analysis of the Southeast Asia monsoons (Cheang, 1987). There is a strong divergent anticyclone over Siberia (cold high) in winter and a convergent cyclone in summer. Therefore, the equatorial pressure trough crosses the equator twice each year corresponding to the north subtropical high and the monsoons over tropical low latitude regions will also change direction twice each year.

In winter, northeasterly winds prevail over the whole South China Sea with an average magnitude of 9 m/s. In summer, southwesterly winds dominate most of the South China Sea and Gulf of Thailand with an average magnitude of 6 m/s (Wyrtki, 1961).

2. Buoyancy Flux at Air-Sea Interface

Rainfall plays a very important role in the South China Sea and the Gulf of Thailand. Figure 7 shows the average rainfall characteristics of the Southeast Asian Waters and Table 2 shows the yearly amounts of precipitation and the other heating properties, where $Q_{eff} - Q_e$ (annual total effective radiation energy - energy required for evaporation) is the available energy for heating processes. The units are: P in cm/yr, E in cm/yr, and $Q_{eff} - Q_e$ in cal/cm^2/day, respectively.

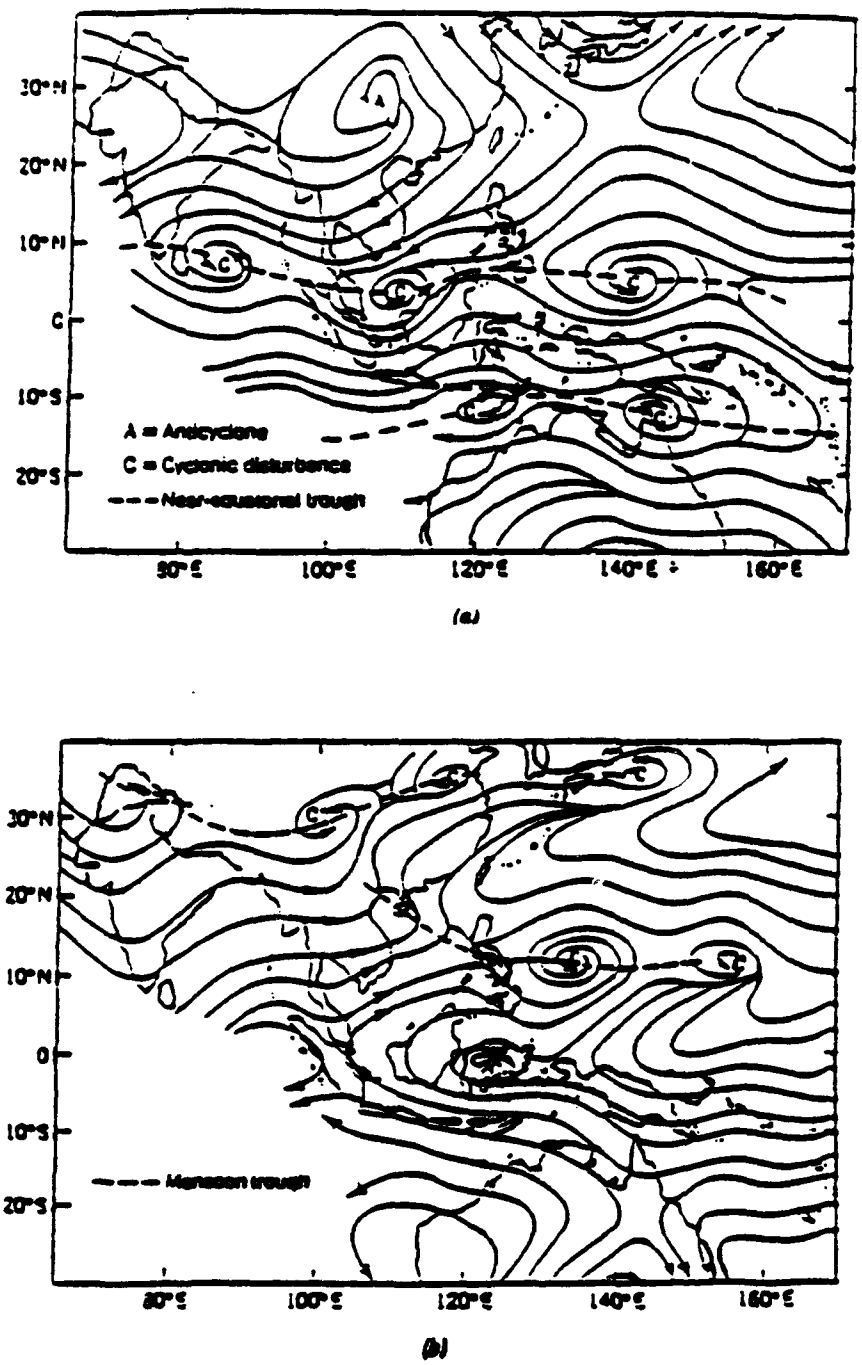

Figure 6 : The Mean 850-mb Streamline of the Southeast Asia Monsoons (a) December, (b) July (Cheang, 1987)

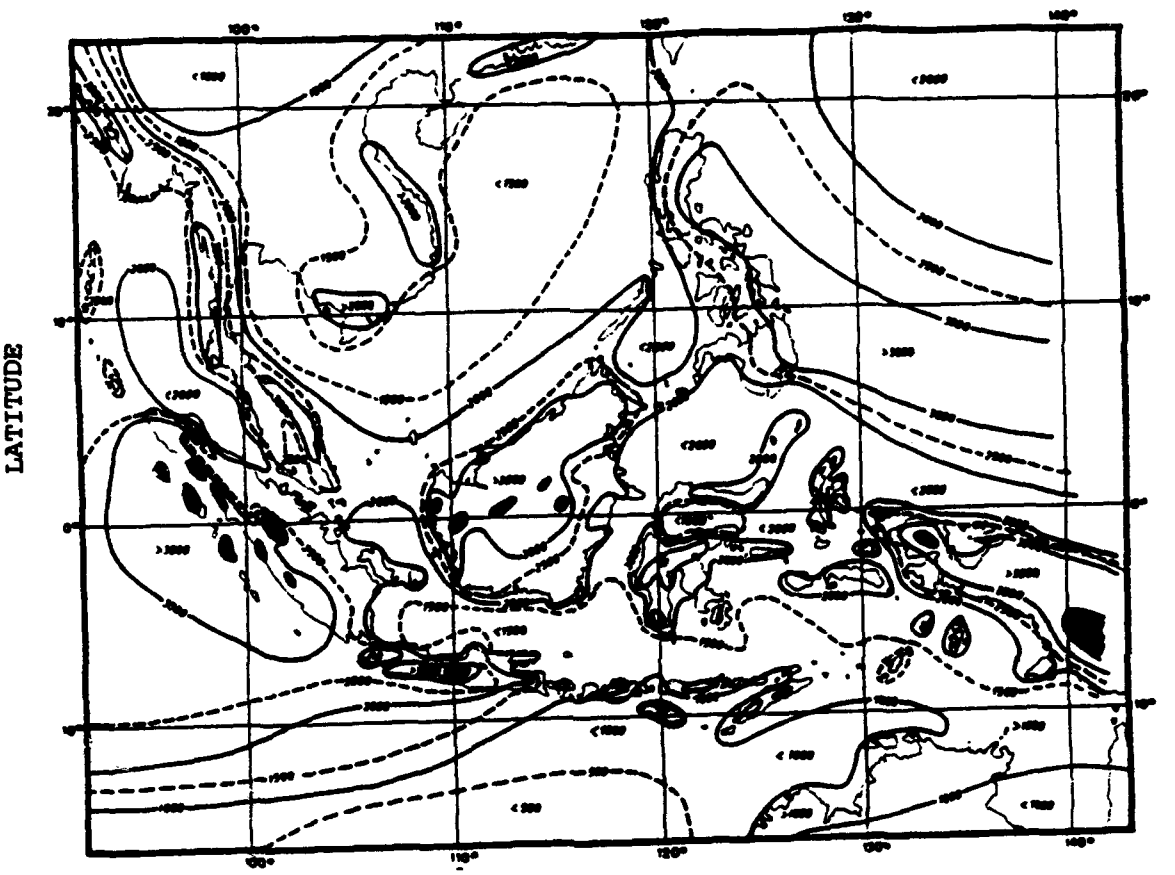

Figure 7 : Average Rainfall (mm/yr) of the Southeast Asian Waters, Higher than 4000 mm Dashed (Wyrtki. 1961)

TABLE 2: THE ANNUAL TOTAL PRECIPITATION AND HEATING PROPERTIES OF THE SOUTHEAST ASIAN WATERS (Wyrtki, 1961)

Regions	Precipitation (cm/yr)	Evaporation (cm/yr)	P - E (cm/yr)	$Q_{eff} - Q_e$ (cal/cm^2/day)
East of Luzon	260	130	130	48
Northern South China Sea	152	133	19	38
Southern South China Sea	221	96	125	100
Java Sea	159	111	48	77
Sulu Sea	180	96	84	107
Strait of Malacca	195	82	113	127
Andaman Sea	200	128	72	56

Heavy rainfall and its strong dependence on latitude are important features of the South China Sea. The precipitation rate decreases from 221 cm/yr in the southern South China Sea to 152 cm/yr in the northern South China Sea. On the other hand, the evaporation rate increases northward from 96 cm/yr in the southern South China Sea to 133 cm/yr in the northern South China sea. The northward increase in evaporation and decrease in precipitation leads to an heterogeneous fresh water influx into the South China Sea surface. The southern South China Sea receives more fresh water (106 cm/yr) than the northern South China Sea. Because of the heavy rainfall and large amounts of energy available for heating, the South China Sea and its adjacent seas are sources of warm, low salinity water (Wyrtki, 1961). According to Table 2, the annual total $Q_{eff} - Q_e$ (cal/cm^2/day) values indicate that the energy available for heating is quite large in the southern South China Sea (100), the Strait of Malacca (127), and the Sulu Sea (107), and quite small in the northern

South China Sea (38), Java Sea (77), and Andaman Sea (56). The north/south difference of the $Q_{eff} - Q_e$ values over the South China Sea is around 62 cal/cm^2/day.

C. OCEANIC CIRCULATIONS

1. The Equatorial Current System

In response to the monsoons and atmospheric features, the wind driven Pacific Ocean equatorial current system has at least four major currents. Three of them extend to the surface, the other remains subsurface. The three major upper layer currents are the westward-flowing North Equatorial Current between about 20° to 8°N, the westward South Equatorial Current from about 3°N to 10°S and the narrow North Equatorial Countercurrent flowing to the east between them. The fourth current, the Equatorial Undercurrent, flows to the east below the surface straddling the equator from about 2°N to 2°S (Pickard and Emery, 1990).

The North Equatorial Current (NEC) flows westward and is divided into two branches off Luzon at 13° to 14°N and they flow southward and northward, respectively (Pickard and Emery, 1990). The southward branch is the Mindanao Current. The northward branch belongs to the Kuroshio Current and flows along the coast of Luzon Island with a maximum velocity of 0.8 - 1.0 m/s, then enters Luzon Strait. After that it turns to the northwest and its main axis reaches as far west as 121°E with a maximum velocity of about 1.5 m/s. There is one branch that often goes westward at 20°N and enters the South China Sea. However, most parts of it will return in the main axis of the Kuroshio Current (Nitani, 1970).

The NEC passes through the passages of the eastern submerged island margin of the South China Sea and mixes with the South China Sea water masses. Bashi Channel in the Luzon Strait is the only passage where the South China Sea waters can exchange with the lower layer and deep ocean water masses of the Pacific Ocean (Wyrtki, 1961). In general, the lower layer water flows in the opposite direction of the surface circulation.

Figure 8 shows the deep water connections between the Pacific and Indian Oceans and the flow of deep waters into the various basins. Deep water enters the South China Sea central deep basin through the Luzon Strait where it branches with one flowing northward into the Palawan Trough and the other flowing out of the South China Sea through the Mindoro Strait. There is no deep water connection between the Sulu Sea and the other deep basin waters. Therefore, the deep water masses in the South China Sea totally belong to the Pacific Ocean water system (Broecker et al., 1986).

2. The Kuroshio Intrusion Through the Luzon Strait

The seasonal variation of the Kuroshio intrusion through the Luzon Strait dominates the structure of water masses of the northern part of the South China Sea. Based on CTD data, Shaw (1989) hypothesized that the intrusion of water from the Kuroshio Current starts in late summer and reaches a maximum in winter. By late spring, the intrusion from the Kuroshio ceases, and the waters from the South China Sea begin to enter the region. Remnants of the intrusion water from the Kuroshio are trapped at the mouth of the Peng-Hu Channel. The water from the South China Sea eventually occupies the entire slope region south of the Peng-Hu Channel until the next intrusion of the Kuroshio begins in late summer.

The intrusion of waters from the Kuroshio could reach at least the salinity minimum layer (about 500 m) and could extend as far north as the Peng-Hu Channel (Shaw, 1989). Because the intrusion water is deep, the steep continental slope poses a strong dynamic constraint to the intrusion current. Consequently, the intrusion water can not continue through the Formosa Strait into the East China Sea. Recent hydrographic data showed that the shelf water in the Formosa Strait was separated from the deep water by a front south of the Peng-Hu Islands in winter. Consequently, it is unlikely that there is a branch of the Kuroshio intrusion in the Formosa Strait.

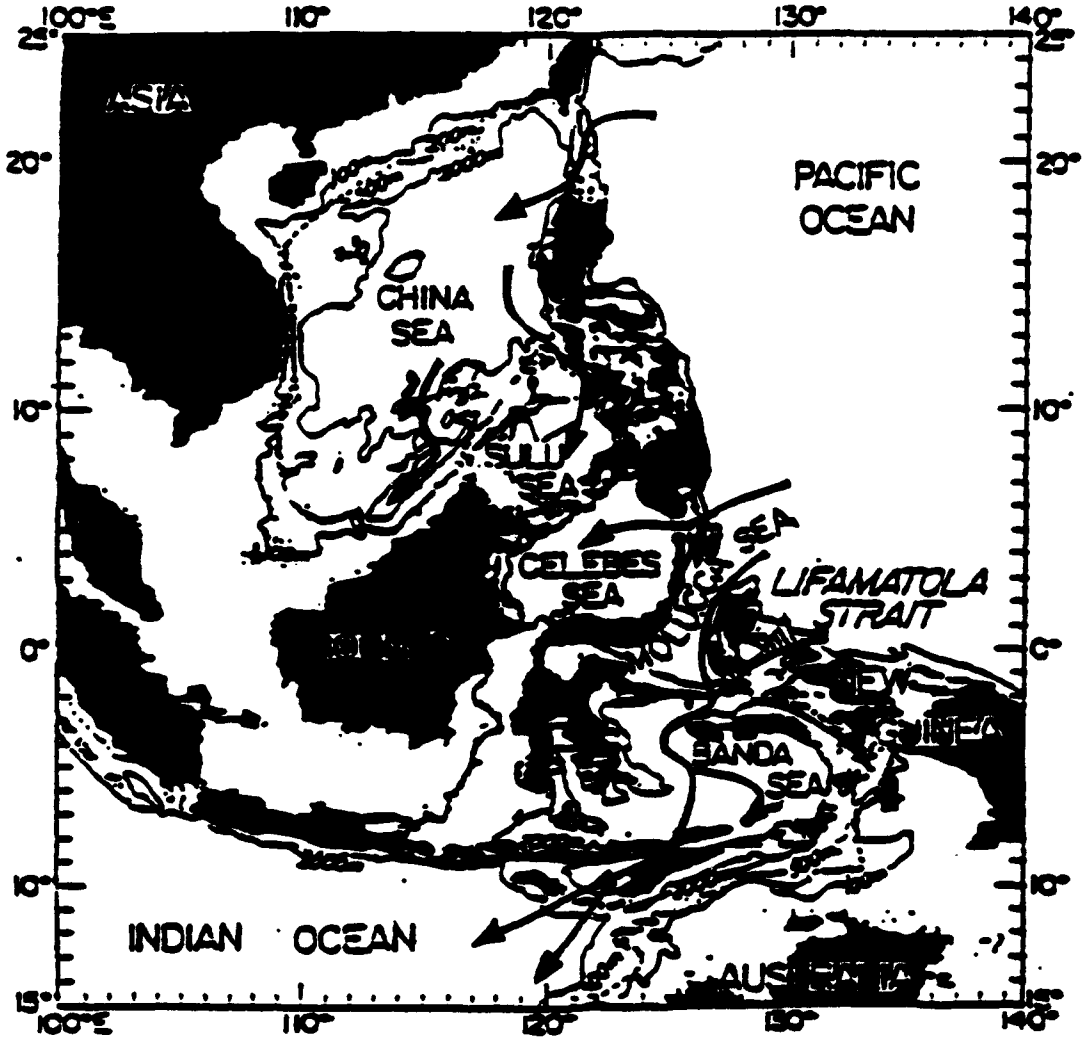

Figure 8 : The Deep Water Connections Between the Pacific and Indian Oceans

(Broecker et al., 1986)

Many studies show that there are anticyclonic and cyclonic circulations on the northern South China Sea near the Luzon Strait (Figure 9). An analysis of the geostrophic current (Zhong, 1990) shows that the anticyclonic circulation at the continental slope consists of the South China Sea Warm Current and the intrusion water of the Kuroshio. A cyclonic eddy is induced periodically by the Kuroshio Current across the Luzon Strait (Liu, 1992). Figure 9 also shows the seasonal variation of the surface current system of the Luzon Strait.

3. The Formosa Strait

The seasonal variation of the current in Formosa Strait is very evident. According to Fan (1982), the current is primarily composed of three different currents: Kuroshio intrusion, the China Coastal Current, and the South China Sea Current. The China Coastal Current originates near the coast of northern China and flows southward along the China coast. When the winter monsoon prevails, it is strengthened by the wind and flows all the way through Formosa Strait and encounters the Kuroshio intrusion at the Peng-Hu Islands.

When the summer monsoon prevails, the South China Sea Current is strengthened and the Kuroshio intrusion is weakened by the southwest winds. Most of the South China Sea current flows through the Luzon Strait while a small amount enters the Formosa Strait flowing northwards. Shaw (1992) found that the cold shelf water in the East China Sea enters the Formosa Strait in fall and winter and also that the coastal discharge from the Yangtze River and rivers south of it produce a southward current into the Formosa Strait.

4. The Java Sea

The Java Sea is smaller than the South China Sea and the currents occupy its full width without the development of larger eddies and counter currents. From May to September the water flows to the west and from November to March to the east. In April

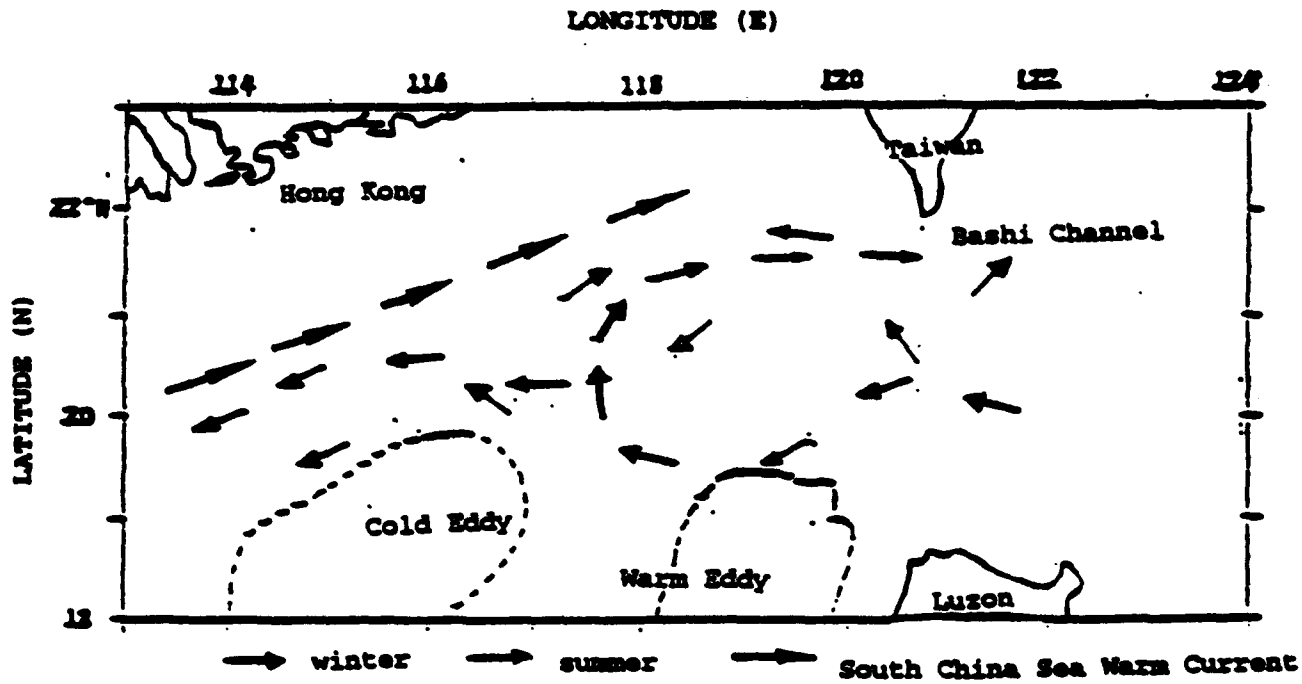

Figure 9 : Seasonal Variation of the Current System Near the Luzon Strait

(Huang, 1988)

and October the direction of the flow reverses and eddies occur. Normally in these months a current towards the east prevails off the coast of Borneo. In the small passages between Borneo and Sumatra, the winds are fresh and the speeds of the currents often reach 1 m/s, especially during the full north monsoon (Wyrtki,1961).

5. The Strait of Malacca

Through the Strait of Malacca a small exchange of water is possible between the Sunda Shelf and the Indian Ocean. The water movements are in general directed towards the Indian Ocean and are strongly related to the surface gradient of the sea level through this strait. In the Strait of Malacca the period of stronger flow is from January to April, during the northeast monsoon, but it is chiefly caused by the low sea level in the Andaman Sea in this season (Wyrtki, 1961).

6. The Gulf of Thailand

Very few observations have been made in the Gulf of Thailand but from available data (Wyrtki, 1961) water movements seem to be weak. During the summer monsoon season they are anticyclonic and when the winter monsoon prevails they are cyclonic. Neelsasri (1979) found that density forcing is as important in driving the circulation as the mechanical forcing of a uniform wind field. He also reports that the currents of the South China Sea induce a shear flow near the open side of the Gulf and that they are confined to the outer half of the Gulf.

7. The South China Sea

The circulation of the South China Sea is mainly determined by the monsoons and the configuration of the land masses surrounding the sea. The ship drift currents of the summer and winter monsoon seasons are shown in Figures 3A and 3B (Wyrtki, 1961), respectively, and summarized as follows.

In June, the largest part of the South China Sea water masses pass south of Taiwan into the root of the Kuroshio; a smaller part flows northwards through the Formosa Strait

joining the Kuroshio Current. Because the supply of water to this current from the Java Sea seems to be insufficient (Wyrtki, 1961), a current develops off the coast of Borneo towards the southwest with a current speed between 0.12 m/s and 0.25 m/s, which turns back to the north in the region of Natuna Island. The water of this current comes partly out of the Sulu Sea, and partly from a counter current, which is formed in the central parts of the South China Sea. This current must develop in close connection with the westward intensification of the main current and be caused dynamically (Wyrtki, 1961). Along the western coast of Luzon water flows northward from the Sulu Sea with a surface current speed of between 0.12 m/s and 0.25 m/s. The surface current speed is more than 1.0 m/s off the coast of Vietnam (Wyrtki, 1961) and about 0.5 m/s off the Hainan coast. In the Gasper and Karimata Straits, the surface current speed is about 0.75 m/s and the current speed of the jet current which flows from Vietnam to the Luzon Strait is about 0.25 m/s to 0.30 m/s during this season.

In December, the northeast monsoon is fully developed over the South China Sea and the currents are strong. Waters from the Kuroshio Current and the East China Sea enter the South China Sea flowing southwestward along the coastline of Asia and flow out of the South China Sea through the Gasper and Karimata Straits. The surface current speeds are about 0.50 m/s off the coast of Hainan, about 0.75 m/s off the coast of Vietnam, and about 0.30 m/s in the Gasper Strait. The westward intensification is stronger than during the southwest monsoon, when a deflection of the current occurs to the east caused by the wind. The counter current in the center of the South China Sea is present and lies farther to the east because of the strength of the main current. From the Sulu Sea water flows into the South China Sea and is mixed into the main current. A current boundary exists between Vietnam and Borneo and a very weak (less than 0.12 m/s) southwestward flow occurs along the coast of Borneo which encounter the waters from the north flowing northward along the right hand side of the current boundary.

D. WATER MASSEES

1. Mass Transport

Wyrtki (1961) showed that on the western side of the Luzon Strait the water masses can be divided into the warm, less saline surface layer water, the high salinity (34.8 -35.2 psu) Subtropical Lower Water, the low salinity (34.1-34.5 psu) Intermediate Waters, and the original Pacific Deep Water (34.65-34.7 psu). The salinity maxima of the Subtropical Lower Water is about 150 m deep and the salinity minima of the Intermediate Waters is about 400 to 500 m deep. According to Wyrtki (1961), in the Luzon Strait these two water masses move in opposite directions and the depth of this inversion is about 200 m. The center of this inversion lies relatively uniformly at a temperature 16°C.

Wyrtki (1961) also found that during the winter monsoon season surface water from the Pacific Ocean is transported into the South China Sea through the Luzon Strait. The vertical extent of this layer is about 200 m. This Subtropical Lower Water spreads chiefly along the western side of the South China Sea following the surface currents. Parts of the Intermediate Water flow out of the South China Sea in depths between 400 and 900 m during this season. During the summer monsoon season the conditions are reversed. The surface water flows out of the South China Sea and below about 300 to 400 m water masses flow into the South China Sea.

According to Nitani (1970) the North Pacific Intermediate Water forms the lower part of the Kuroshio Current. The transport of the Kuroshio Current off Luzon is about two-thirds to three-fourths that of the Mindanao Current, which is about 30-45 Sv ($10^6 m^3/s$), and is smaller than that of the Kuroshio Current off the south coast of Japan. Figure 10 shows the mass transport in June and December of the Southeast Asian Waters and Table 3 shows values of mass transports for different currents. According to Table 3, the mass transport of the Kuroshio Current to the east of the Luzon Strait is the largest transport in the area. However, in the South China Sea the largest transport occurs off the Vietnam coast.

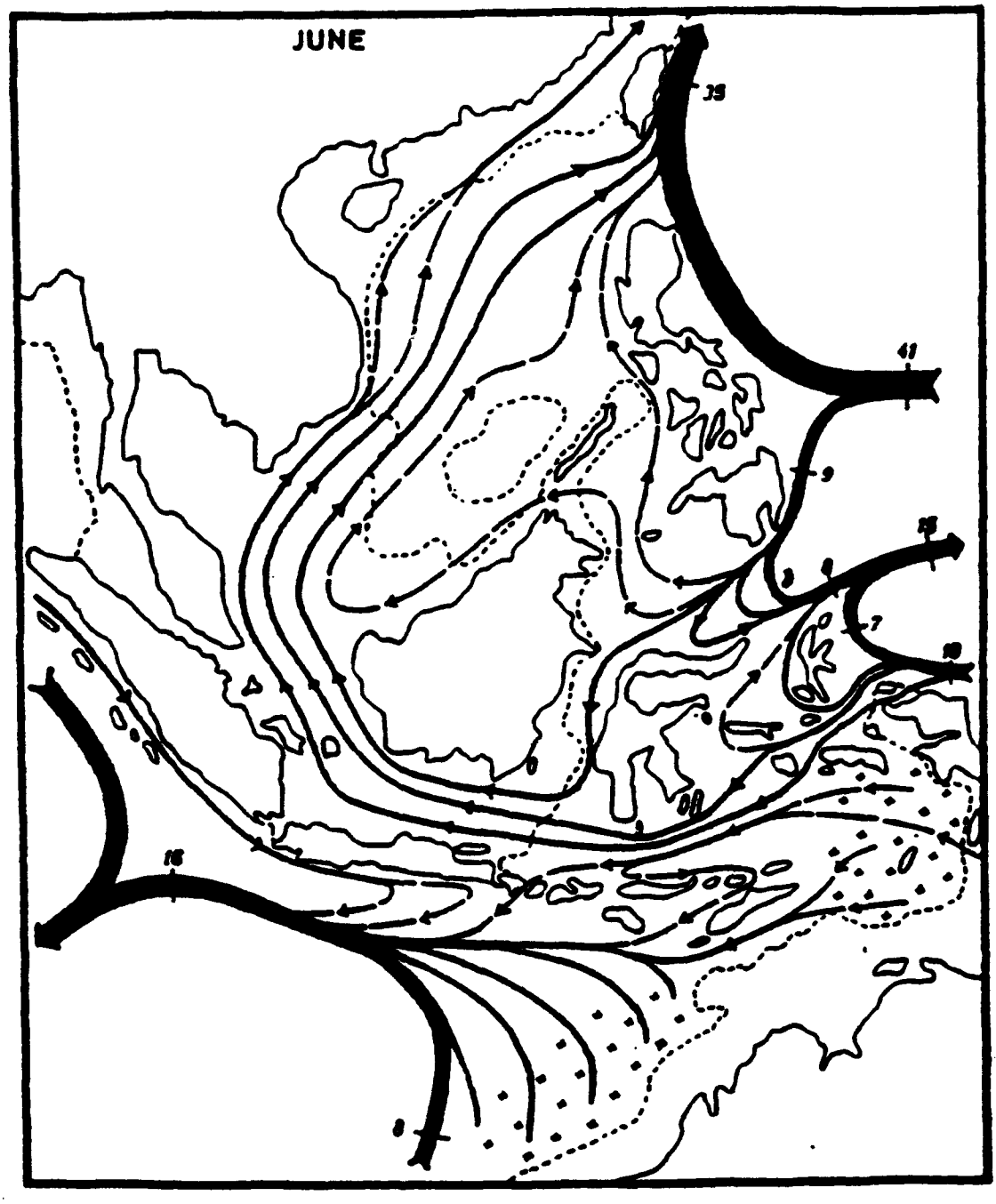

Figure 10A : Summer (June) Mass Transport (Sv) of the Southeast Asian Waters

(Wyrtki, 1961)

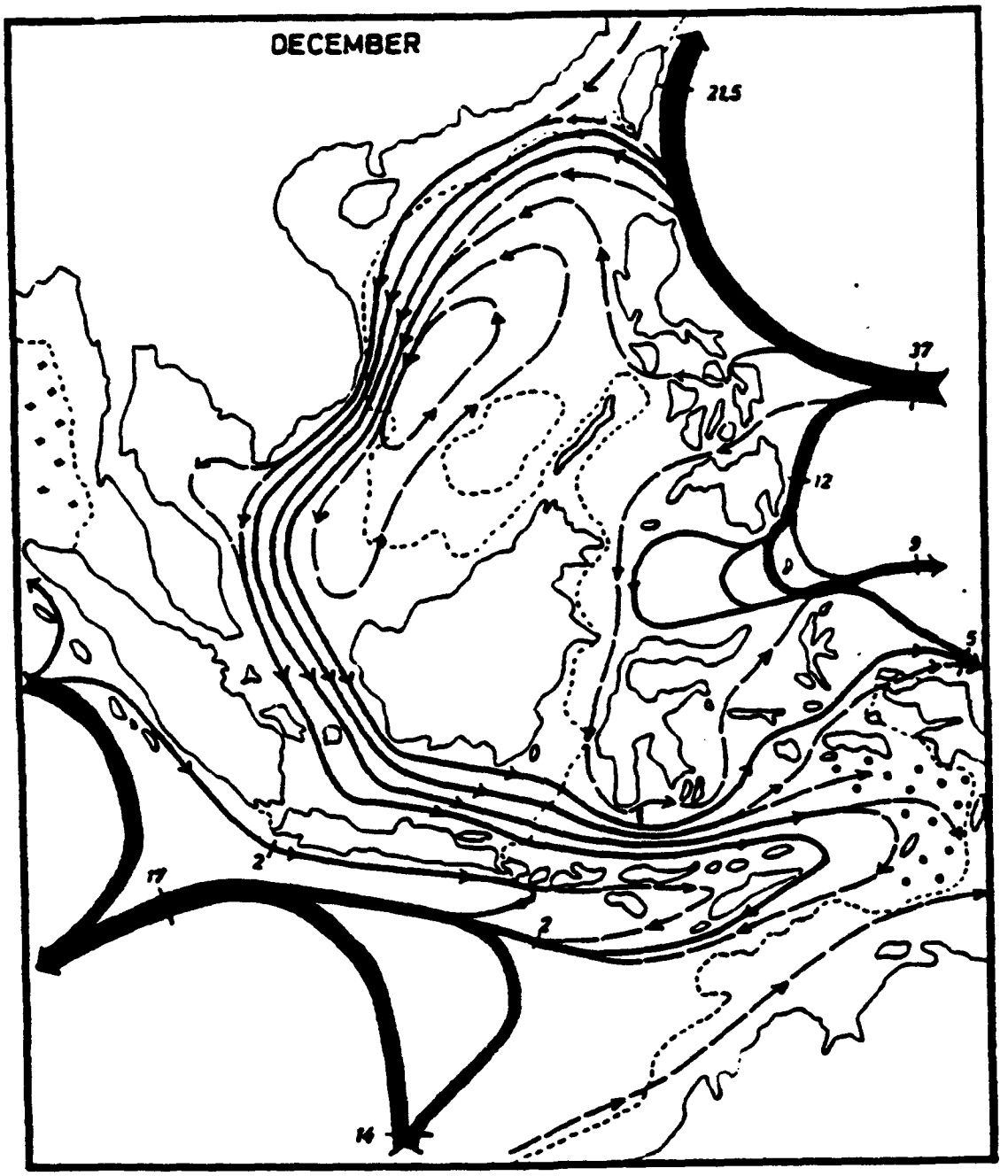

Figure 10B : Winter (December) Mass Transport (Sv) of the Southeast Asian Waters

(Wyrtki, 1961)

TABLE 3: MASS TRANSPORT (Sv) OF CURRENTS IN THE SOUTHEAST ASIAN WATERS (Wyrtki, 1961)

Currents	Feb.	Apr.	Jun.	Aug.	Oct.	Dec.
Kuroshio Current (Northwards positive)	24.5	37.5	35.0	30.5	27.0	21.5
Off Vietnam Current (Southwards Positive)	5.0	1.5	-3.5	-3.0	2.0	5.0
Timor Current (Westwards positive)	1.0	1.5	1.0	1.5	1.5	1.5
Luzon Strait Current (Westwards Positive)	2.5	0	-3.0	-2.5	0.5	3.0

2. Temperature and Salinity

According to Liahude (1979) during the winter monsoon season the northeast monsoon brings cool (about 26°C), high salinity (about 33.5 psu) water from the northern South China Sea into the southern South China Sea. During the summer monsoon season the southwest monsoon brings warm (about 29°C), low salinity (32.5 psu) water from the Java Sea into the southern South China Sea. The waters in the southern South China Sea and the Java Sea are warm and less saline. Thus, the variations of water properties in the South China Sea are mainly determined by the cool, high salinity waters from the north in the winter monsoon season. On the other hand, the river runoff plays an important role in determining the surface salinity in the Gulf of Thailand, the Gulf of Tonkin, and the regions around Borneo (Wyrtki, 1961). Large salinity gradients also exist in these regions.

The Levitus (1982) surface temperature distributions in the South China Sea for summer and winter are shown in Figures 11A (June), 11B (December), and seasonal surface salinity in Figures 12A (June), and 12B (December).

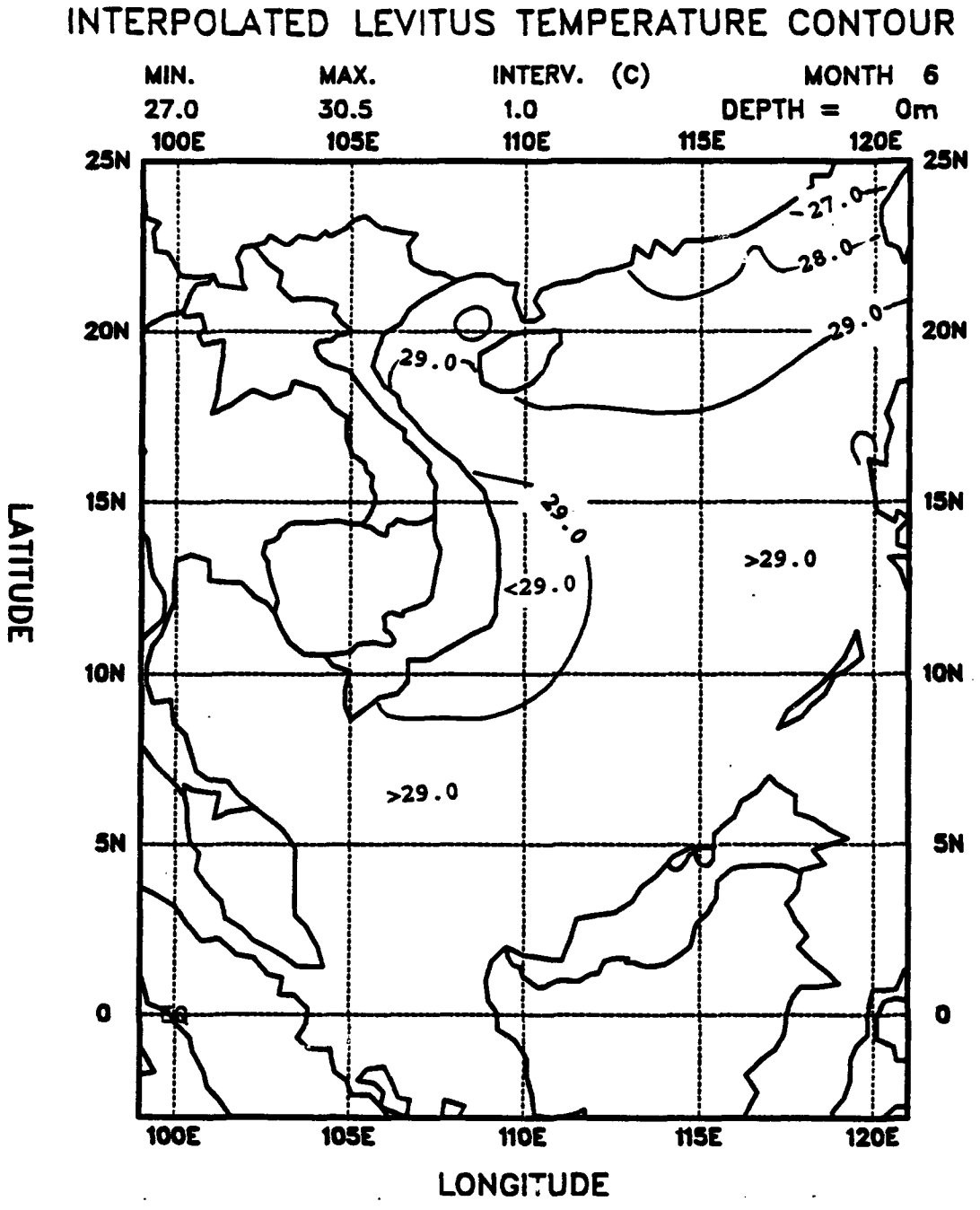

Figure 11A : Levitus Surface Temperature Distribution (June); Interval = 1°C

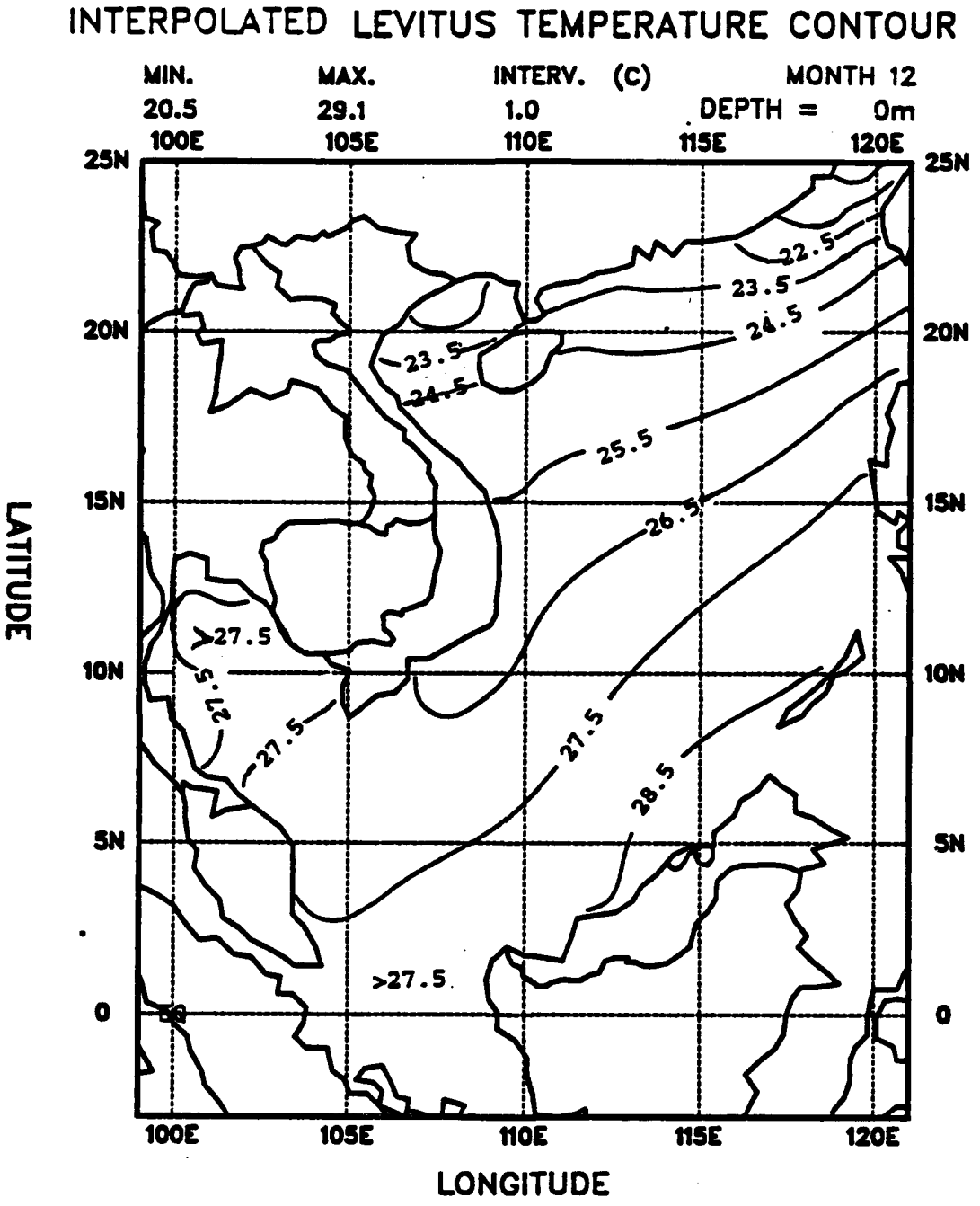

Figure 11B : Levitus Surface Temperature Distribution (December); Interval = 1°C

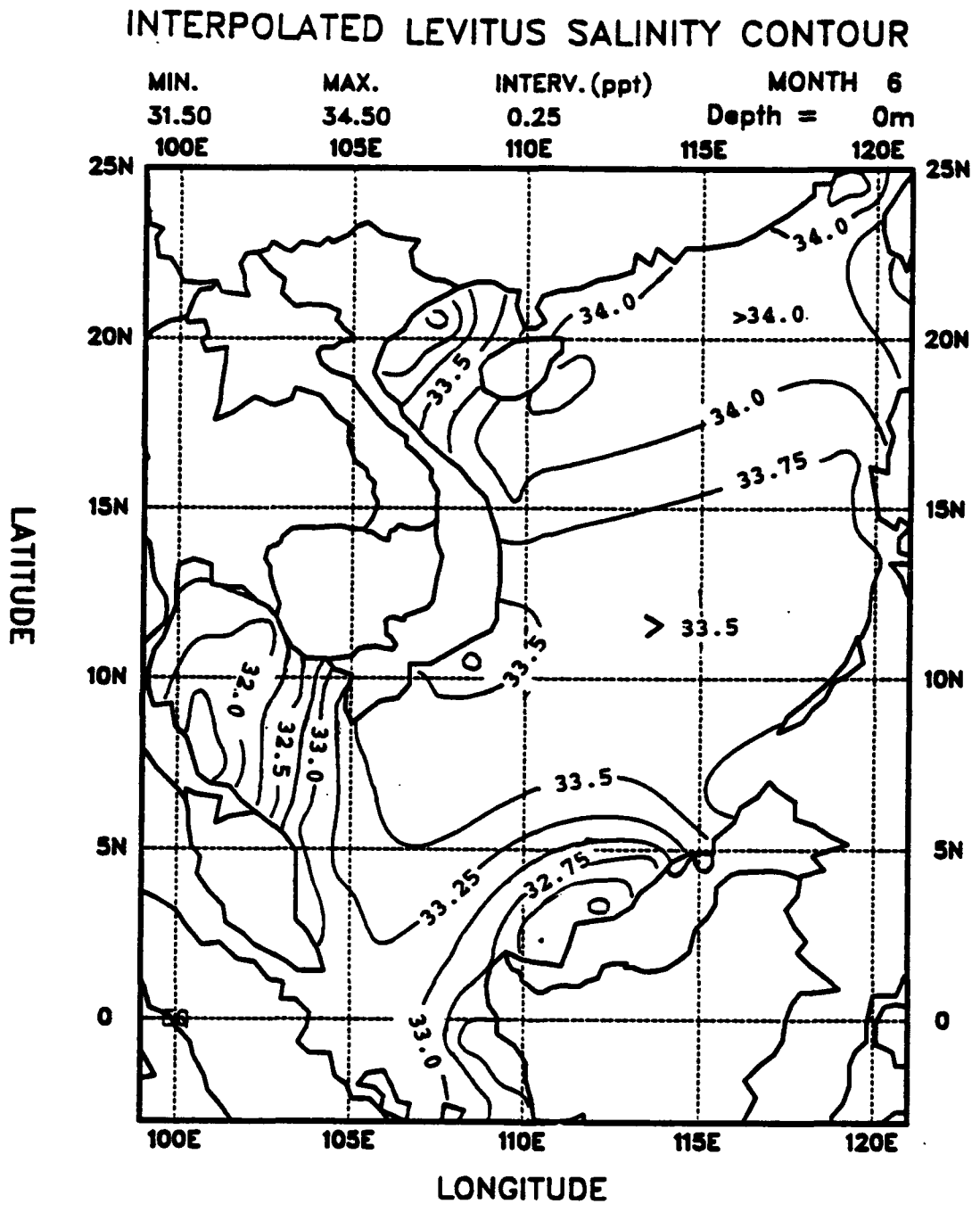

Figure 12A : Levitus Surface Salinity Distribution (June); Interval = 0.25 psu

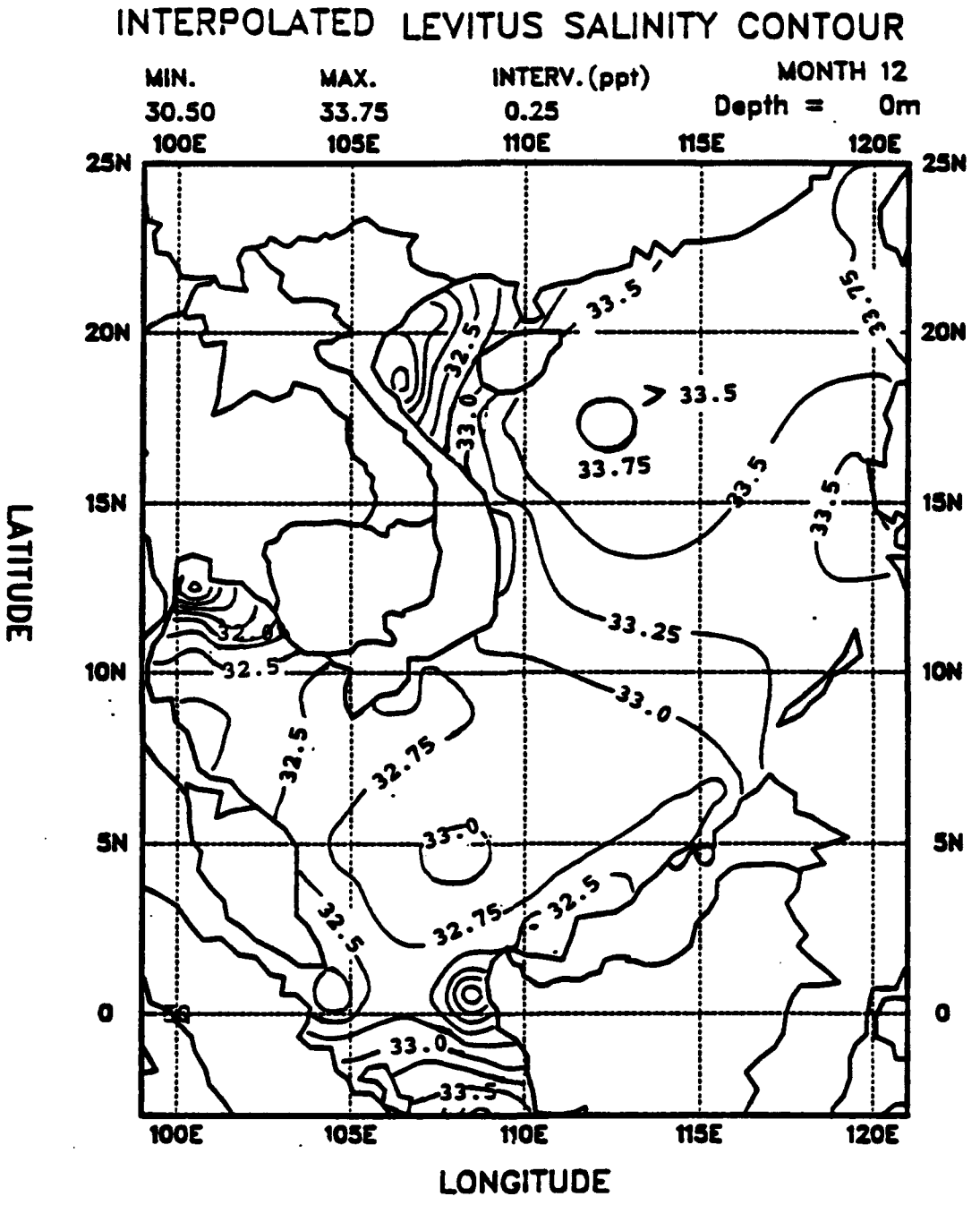

Figure 12B : Levitus Surface Salinity Distribution (December); Interval = 0.25 psu

Summer: In June (Figure 11A) surface temperature is homogeneous (about 29°C) in most part of the South China Sea, except in the Gulf of Tonkin and the Formosa Strait. In the Formosa Strait they are between 26.5°C and 28°C.

The surface salinity is between 33.0 psu and 34.0 psu in most parts of the South China Sea (Figure 12A). Exceptions occur in the Formosa Strait, the Gulf of Tonkin, the Gulf of Thailand, and the coast of Borneo. Surface salinities are about 30.5 psu to 32.5 psu in the Gulf of Thailand and 31.5 psu to 33.25 psu in the Gulf of Tonkin, respectively. In the Formosa Strait surface salinity is more than 34.0 psu. Off the coast of Borneo surface salinity is between 32.5 psu and 32.75 psu.

Winter: In December (Figure 11B) the isotherms spread southwestward increasing from 22°C in the Formosa Strait to 28°C off the coast of Borneo. The largest surface temperature gradients occur in the Formosa Strait (20.5°C to 22.5°C). In the Gulf of Thailand the surface temperature is higher than 27.5°C. In the Gulf of Tonkin, however, surface temperatures are between 23.0°C and 25.5°C.

The surface salinity increases with latitude in winter from 33.0 psu in the southern South China Sea to 34.0 psu in its northern reaches (Figure 12B). Large salinity gradients occur in the Gulf of Tonkin, the Gulf of Thailand and the western side of Borneo. In the northern South China Sea, surface salinity is between 33.5 psu and 34.0 psu. In the Gulf of Tonkin and the Gulf of Thailand, surface salinity varies from about 31.0 psu to 33.5 psu. In the southern and central South China Sea, surface salinities are homogeneous between 33.25 psu and 33.5 psu. The surface salinity is more than 33.5 psu in the Gasper and Karimata Straits.

III. NUMERICAL MODEL

A. INTRODUCTION

The Princeton turbulent closure model (Blumberg and Mellor, 1987) was implemented for the South China Sea at the University of Miami and the Naval Postgraduate School. The model grid is shown in Figure 11. The model domain is 99°E - 121°E, 3°S - 25°N which includes the South China Sea and the Gulf of Thailand. With its 20 km horizontal resolution and 23 vertical sigma coordinate levels, it has $125 \times 162 \times 23$ grid points. By using the mode splitting technique and finite difference formulation introduced by Blumberg and Mellor (1987), the governing equations for momentum, heat, and salt can be simplified to predict four different prognostic variables: surface elevation, η, temperature, T, salinity, S, and velocity, (U,V,W).

The data sets needed in this simulation are bathymetry, surface wind stress, temperature, salinity, and mass transport at the lateral open boundaries. NAVOCEANO dbdb5 bathymetry, Hellerman wind stress, and Levitus temperature/salinity data sets are available for this modeling research. The original data resolutions are as follows.

* NAVOCEANO dbdb5 Bathymetry ($5' \times 5'$)
* Monthly Levitus temperature/salinity ($1° \times 1°$; 19 levels).
* Annual Levitus temperature/salinity ($1° \times 1°$; 33 levels).
* Monthly Hellerman wind stress ($2° \times 2°$).

All the data used in this simulation were interpolated into the model grids.

Since the Levitus monthly data sets only have 19-levels, the data below the 19th-level (levels 20-33) were taken from the mean annual climatological Levitus data. Here, a data smoothing technique was used to prevent an unrealistic jump between the 19th and the lower levels.

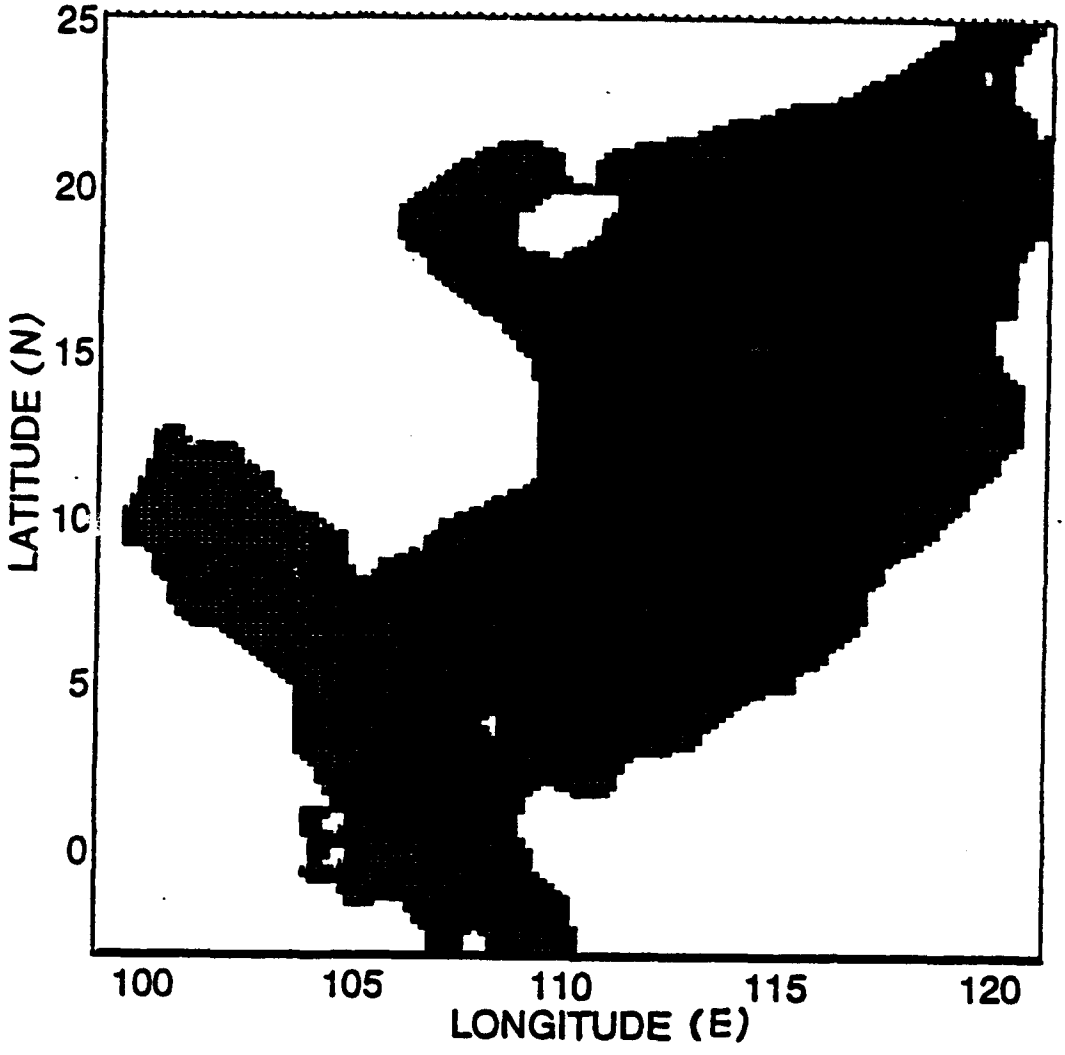

Figure 13 : Model Grid

Hellerman and Rosenstein (1983) used a quadratic bulk aerodynamic formulation to calculate the surface wind stresses. Over 35 million oceanic surface observations exist, extending from 1870 to 1976 and archived by the National Climatic Center in Asheville, NC, designated TDF-11, and grouped into data set with $2^{\circ} \times 2^{\circ}$ resolution.

B. MODEL FEATURES

The model features are listed as the follows:

* Primitive equation model.
* Second order turbulent closure.
* σ coordinate (vertical).
* Curvilinear orthogonal coordinates (horizontal).
* Free surface.
* Split time steps (internal mode = 900 sec.; external mode = 25 sec.)
* No slip hard boundary conditions.
* No fluxes on rigid boundaries (bottom, side walls).

C. MODEL GOVERNING EQUATIONS

According to Blumberg and Mellor (1987), this model uses the implicit numerical scheme in the vertical direction and a mode splitting technique in time which has been adopted for computational efficiency and which separates the external mode (vertically integrated equations) from the internal mode (vertical structure equations). Its numerics will accommodate the highly time-dependent and often nonlinear processes of coastal upwelling and eddy dynamics. By using the hydro-statistic and Boussinesq assumptions and considering a system of orthogonal Cartesian coordinates with x increasing eastward, y increasing northward, and z increasing upward, the governing equations of this model, which form the basis of the circulation model, describe the velocity and surface elevation fields, and the salinity and temperature fields.

The free surface is located at $z = \eta(x, y, t)$ and the bottom boundary is at $z = -H(x, y)$. The $\vec{V}$ is the horizontal velocity vector with components (U, V) and ∇ is the horizontal gradient operator.

1. The Continuity Equation

$$\nabla \cdot \vec{V} + \frac{\partial W}{\partial z} = 0 \qquad (1)$$

2. The Momentum Equations

$$\frac{\partial U}{\partial t} + \vec{V} \cdot \nabla U + W\frac{\partial U}{\partial z} - fV = -\frac{1}{\rho_0}\frac{\partial P}{\partial x} + \frac{\partial}{\partial z}(K_M\frac{\partial U}{\partial z}) + F_x \qquad (2a)$$

$$\frac{\partial V}{\partial t} + \vec{V} \cdot \nabla V + W\frac{\partial V}{\partial z} + fU = -\frac{1}{\rho_0}\frac{\partial P}{\partial y} + \frac{\partial}{\partial z}(K_M\frac{\partial V}{\partial z}) + F_y \qquad (2b)$$

$$\rho g = -\frac{\partial P}{\partial z} \qquad (2c)$$

with ρ_0 the reference density, ρ the in situ density, g the gravitational acceleration, P the pressure, K_M the vertical eddy diffusivity of turbulent momentum mixing, and f the Coriolis parameter.The pressure at depth z is:

$$P(x, y, z, t) = P_{atm} + g\rho_0\eta + g\int_z^0 \rho(x, y, z', t)\, dz'$$

where η is the free surface and the atmosphere pressure, P_{atm}, is assumed constant.

3. The Conservation Equations for Temperature and Salinity

$$\frac{\partial \theta}{\partial t} + \vec{V} \cdot \Delta\theta + W\frac{\partial \theta}{\partial z} = \frac{\partial}{\partial z}(K_H\frac{\partial \theta}{\partial z}) + F_\theta \qquad (3a)$$

$$\frac{\partial S}{\partial t} + \vec{V} \cdot \nabla S + W\frac{\partial S}{\partial z} = \frac{\partial}{\partial z}(K_H\frac{\partial S}{\partial z}) + F_S \qquad (3b)$$

where θ is the potential temperature (or in situ temperature for shallow water applications) and S is the salinity. The density is computed by using the equation of state of the form $\rho = \rho_p(\theta, S)$ where ρ_p is the potential density. K_H denotes the horizontal eddy diffusivity for turbulent mixing of heat and salt.

All of the motions induced by small-scale processes not directly resolved by the model grid are parameterized in terms of horizontal mixing processes. These unsolved processes are denoted by F terms in the following equations

$$F_x = \frac{\partial}{\partial x}(2A_M\frac{\partial U}{\partial x}) + \frac{\partial}{\partial y}(A_M(\frac{\partial U}{\partial y} + \frac{\partial V}{\partial x})) \tag{4a}$$

$$F_y = \frac{\partial}{\partial y}(2A_M\frac{\partial V}{\partial y}) + \frac{\partial}{\partial x}(A_M(\frac{\partial U}{\partial y} + \frac{\partial V}{\partial x})) \tag{4b}$$

$$F_{\theta,S} = \frac{\partial}{\partial x}(A_H\frac{\partial}{\partial x}(\theta, S)) + \frac{\partial}{\partial y}(A_H\frac{\partial}{\partial y}(\theta, S)) + R_{\theta,S} \tag{4c}$$

where A_M and A_H are the horizontal diffusivities, which are the horizontal turbulent exchange coefficients for momentum and heat/salt mixing and the atmospheric thermodynamic forcing, respectively. $R_{\theta,S}$ is the term representing relaxation to the Levitus temperature and salinity. Although the F terms allow variable coefficients, their values as low as $10\,(m^2/s)$ have been used successfully in various applications. We use the Smagorinsky diffusivity for horizontal diffusion and its formula is:

$$A_M = 0.1\,(\Delta x \Delta y)\,((\frac{\partial U}{\partial x})^2 + 0.5\,(\frac{\partial V}{\partial x} + \frac{\partial U}{\partial y})^2 + (\frac{\partial V}{\partial y})^2)^{\frac{1}{2}}.$$

D. TURBULENCE CLOSURE

The vertical mixing coefficients, K_M and K_H in (5a),(5b),(6a),(7a) are determined by the second order turbulence closure scheme (Blumberg and Mellor, 1987). According to (5a) and (5b), they will be characterized by equations for turbulent kinetic energy (TKE), $q^2/2$, and the turbulence macroscale (turbulence mixing length), l.

$$\frac{\partial q^2}{\partial t} + \vec{V}\cdot\nabla q^2 + W\frac{\partial q^2}{\partial z} = \frac{\partial}{\partial z}(K_q\frac{\partial q^2}{\partial z}) + 2K_M((\frac{\partial U}{\partial z})^2 + (\frac{\partial V}{\partial z})^2) + \frac{2g}{\rho_0}K_H\frac{\partial \rho}{\partial z} - \frac{2q^3}{B_1 l} + F_q \tag{5a}$$

$$\frac{\partial lq^2}{\partial t} + \vec{V}\cdot\nabla lq^2 + W\frac{\partial 2lq^2}{\partial z} = \frac{\partial}{\partial z}(K_q\frac{\partial lq^2}{\partial z}) + lE_1K_M((\frac{\partial U}{\partial z})^2 + (\frac{\partial V}{\partial z})^2) + \frac{lE_1 g}{\rho_0}K_H\frac{\partial \rho}{\partial z} - \frac{2q^3}{B_1}\tilde{W} + F_l \tag{5b}$$

where $\tilde{W} = 1 + E_2 (\frac{l}{\kappa L})^2$ is the wall proximity function and L can be calculated by $L^{-1} = (\eta - z)^{-1} + (H + z)^{-1}$. Near the surfaces the Von Karman constant $\kappa = 0.4$, and thus $l/\kappa \sim L$, $\tilde{W} = 1 + E_2$, and far from the surface $l \ll L$, $\tilde{W}^2 \cong 1$. The first term on the right hand side of (5a),(5b) is diffusion, the next two terms are shear production and horizontal mixing. The horizontal mixing terms, F_q and F_l, can be parameterized analogously to temperature and salinity by using (4a),(4b). The vertical mixing coefficients (K_M, K_H, and K_q) are determined from $K_M = lqS_m$, $K_H = lqS_h$, $K_q = lqS_q$, where S_m, S_h, and S_q are stability functions that are analytically derived and depend on variables $\frac{\partial U}{\partial z}$, $\frac{\partial V}{\partial z}$, and $\frac{\partial \rho}{\partial z}$, q, ρ_{0g}, and l.

E. SURFACE AND BOTTOM BOUNDARY CONDITIONS

The boundary conditions at the free surface ($z = \eta(x, y)$) are:

$$\rho_0 K_M (\frac{\partial U}{\partial z}, \frac{\partial V}{\partial z}) = (\tau_{0x}, \tau_{0y}) \tag{6a}$$

$$q^2 = B_1^{\frac{2}{3}} U_{\tau S}^2 \tag{6b}$$

$$q^2 l = 0 \tag{6c}$$

$$W = U\frac{\partial \eta}{\partial x} + V\frac{\partial \eta}{\partial y} + \frac{\partial \eta}{\partial t} \tag{6d}$$

where (τ_{ox}, τ_{0y}) is the surface wind stress vector and $U_{\tau S}$ is the magnitude of the ocean surface friction velocity. $B_1^{\frac{2}{3}}$ is an empirical constant arising from the turbulence closure relations. On the bottom and the side walls of the basin, the normal gradients of θ and S are zero. No energy flux could pass through these boundaries. The boundary conditions at the bottom ($z = -H(x, y)$) are:

$$\rho_0 K_M \left(\frac{\partial U}{\partial z}, \frac{\partial V}{\partial z}\right) = (\tau_{bx}, \tau_{by}) \tag{7a}$$

$$q^2 = B_1^{\frac{2}{3}} U_{\tau b}^2 \tag{7b}$$

$$q^2 l = 0 \tag{7c}$$

$$W_b = (-U_b)\frac{\partial H}{\partial x} - V_b \frac{\partial H}{\partial y} \tag{7d}$$

where the $-H(x, y)$ is the bottom topography and $U_{\tau b}$ is the bottom friction velocity associate with the bottom frictional stresses (τ_{bx}, τ_{by}). According to the logarithmic law, the bottom stresses can be calculated by the equation:

$$\vec{\tau}_b = \rho_0 C_D |\vec{V}_b| \vec{V}_b$$

The drag coefficient, C_D, is determined by the equation:

$$C_D = \left(\frac{1}{\kappa} \frac{ln(H + z_b)}{z_0}\right)^{-2}$$

where $z_0 = 0.01\,\text{m}$ and $C_D = 0.0025$ are recommended by Blumberg and Mellor (1987) and will be used in this simulation. z_b and $\vec{V}_b$ are the grid point and the corresponding velocity in the grid point nearest the bottom, respectively. If enough resolution data is provided and associated with the turbulent-closure-derived K_M, the velocity in the lower boundary region can be calculated by the equation:

$$\vec{V} = \left(\frac{\vec{\tau}_b}{\kappa U_{\tau b}}\right) ln\left(\frac{z}{z_0}\right).$$

The value of roughness length, z_0, depends on the local bottom roughness.

F. σ COORDINATE SYSTEM

In this simulation the sigma coordinate system is used. The governing external and internal mode equations are transformed from (x,y,z,t) to $(\dot{x}, \dot{y}, \sigma, \dot{t})$coordinates,

$$\dot{x} = x, \dot{y} = y, \sigma = \frac{z - \eta}{H + \eta}, t = \dot{t}$$

and the σ ranges from σ = 0 at $z = \eta$(surface) to σ = -1 at $z = -H$ (bottom). Thus, all the derivatives in the dynamic equations will be transformed from the Cartesian coordinate system to the new system and used in this modeling research. By using a cubic spline interpolation, the sigma coordinate values and the Cartesian coordinate values can be transformed to each other as needed.

G. INITIAL CONDITIONS

The model is integrated from 30 April (t=0). The initial conditions of the model are

$$U = 0, V = 0, W = 0$$

$$T = T|_{t=0}$$

$$S = S|_{t=0}$$

where $T|_{t=0}$, $S|_{t=0}$ are the temperature and salinity on 30 April, which are obtained by interpolating the Levitus monthly data.

H. OPEN BOUNDARY CONDITIONS

A lateral open boundary is any place where the water can flow through. The mass transports through the Strait of Malacca, Banka Strait, Balabac Strait, and Mindoro Strait are quite weak. Therefore, for simplicity, these straits are kept closed in the model simulation. The three other boundaries are remain open, the Luzon Strait, Formosa Strait, Karimata and Gasper Straits. The water mass properties (temperature and salinity) are given according to the monthly Levitus data. The bi-monthly specified mass transports are given in Table 4.

TABLE 4: MONTHLY MASS TRANSPORT (Sv) AT THE OPEN BOUNDARIES

Month	Feb.	Apr.	Jun.	Aug.	Oct.	Dec.
Gasper&Karimata Straits (Eastwards Positive)	4.4	0.0	-4.0	-3.0	1.0	4.3
Luzon Strait (Eastwards Positive)	-3.5	0.0	3.0	2.5	-0.6	-3.4
Formosa Strait (Northwards Positive)	-0.9	0.0	1.0	0.5	-0.4	-0.9

I. ATMOSPHERIC FORCING

The atmospheric forcing includes wind forcing and thermodynamic forcing. In this simulation the Hellerman wind stress has been used as the wind forcing data. Figure 14 shows the Hellerman wind stress distributions over the South China Sea. In summer, winds from the Indian Ocean and Australia meet at Natuna Island blowing northward and counterclockwise all over the South China Sea. Winds originating from Australia are very weak and extend only to Natuna Island. The air stream from the Indian Ocean is stronger and dominates the atmospheric circulation during this season. The strength of winds in May (Figure 14A) is about five times weaker than in June (Figure 14B). In May, northerly winds can reach up to 20°N where they converge with the southwestward winds from the East China Sea and blow westward from Luzon to Hainan. In June, the prevailing winds over the South China Sea blow northeastward and counterclockwise from Vietnam to the Luzon Strait. In winter, winds from the Pacific Ocean blow southwestward from Taiwan to Singapore and then turn left toward the Java Sea. In November (Figure 14C), winds are as strong as in December (14D), but their southerly extent is limited to 10°N whereas in December they extend to Natuna Island (5°N).

Heat fluxes are very important for the equatorial region. According to Levitus (1982), the South China Sea has an annual mean temperature of 28°C, higher than its adjacent Pacific Ocean waters. Therefore, the South China Sea water is an extensive heat source for the adjacent regions. In this simulation, the relaxation to the Levitus temperature and salinity data were included in the thermodynamic forcing. This prevents any extreme deviation from climatological mean values and guarantees that the South China Sea will act as a heat source.

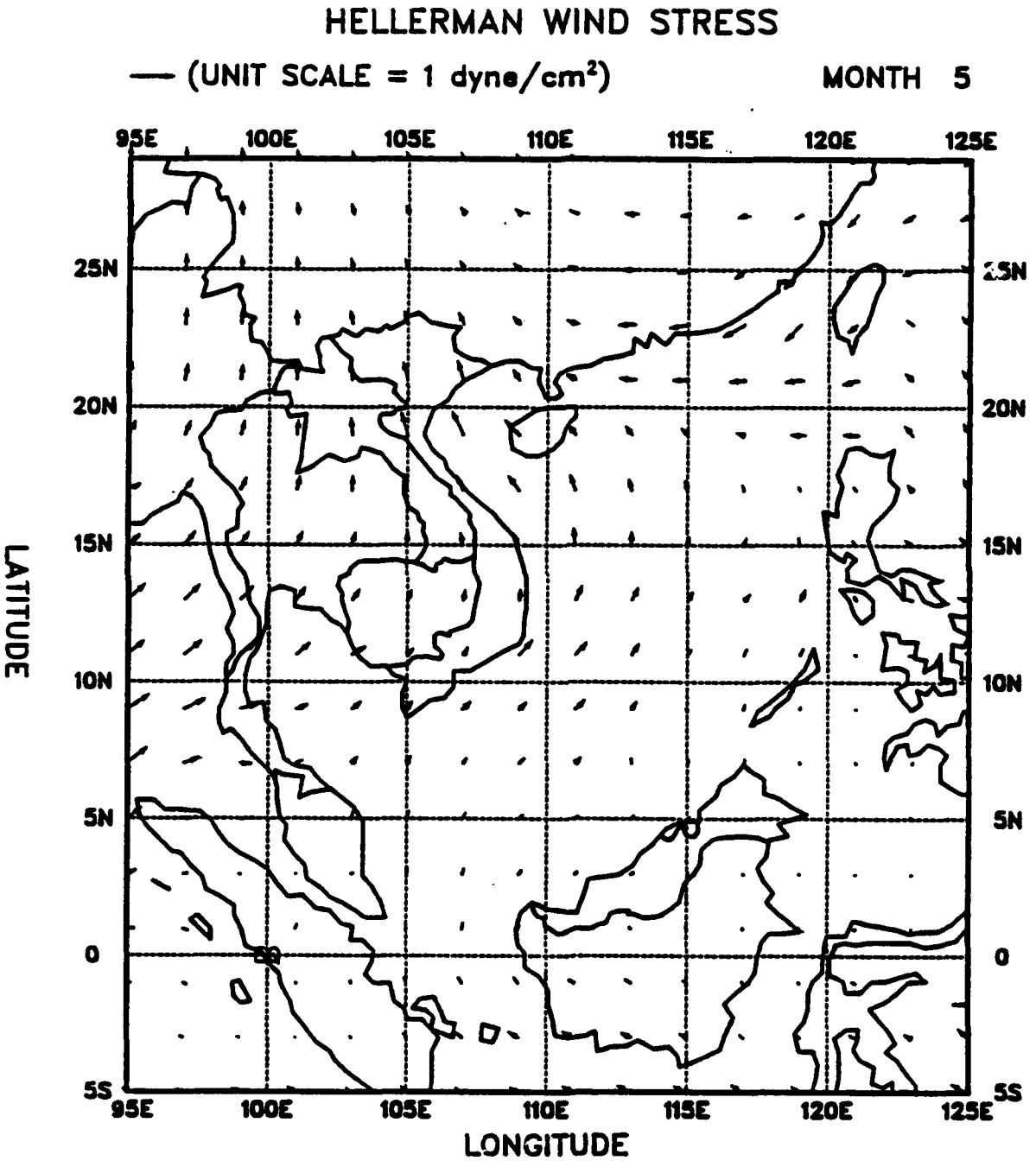

Figure 14A : Summer (May) Hellerman Wind Stress Distribution

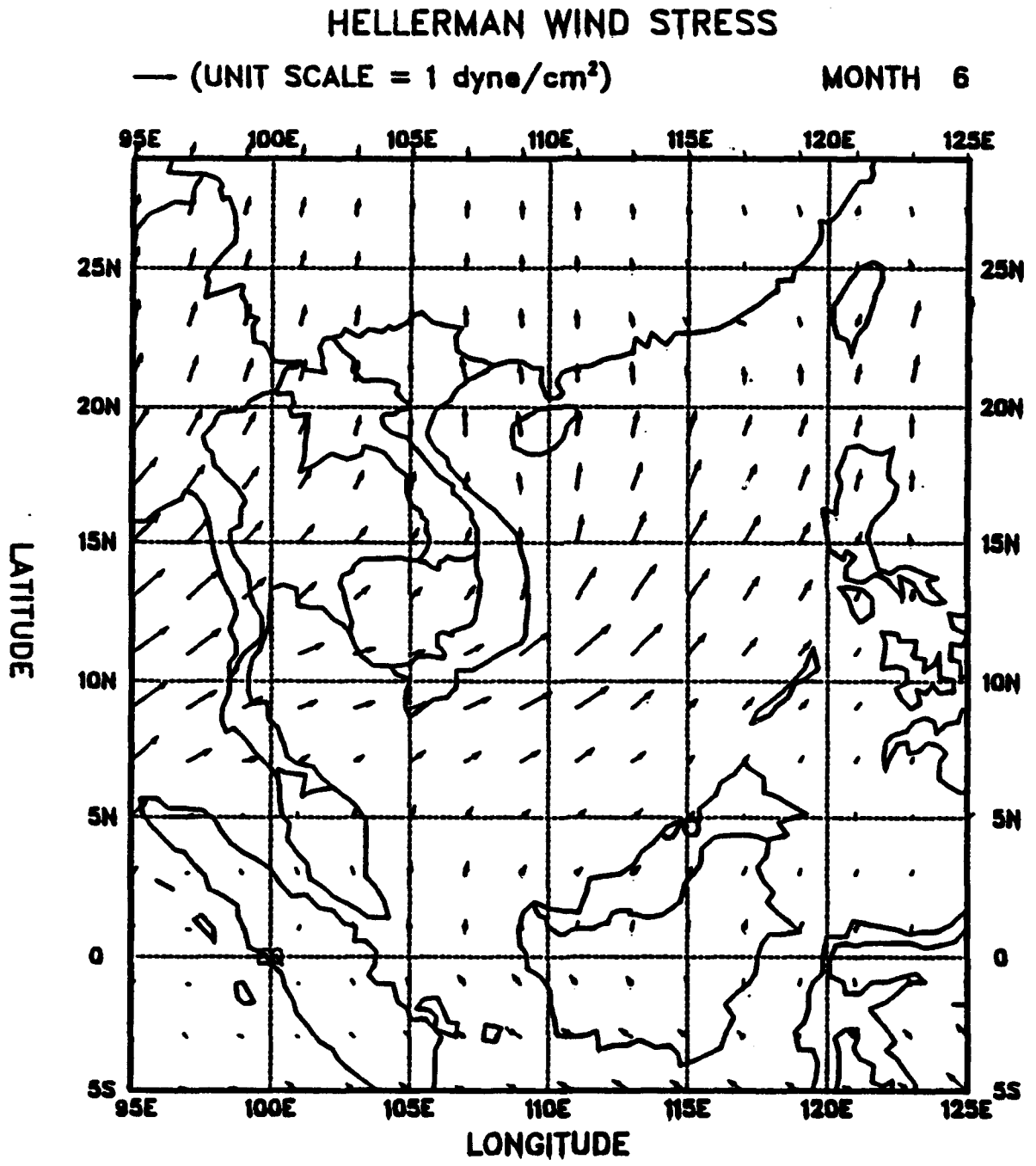

Figure 14B : Summer (June) Hellerman Wind Stress Distribution

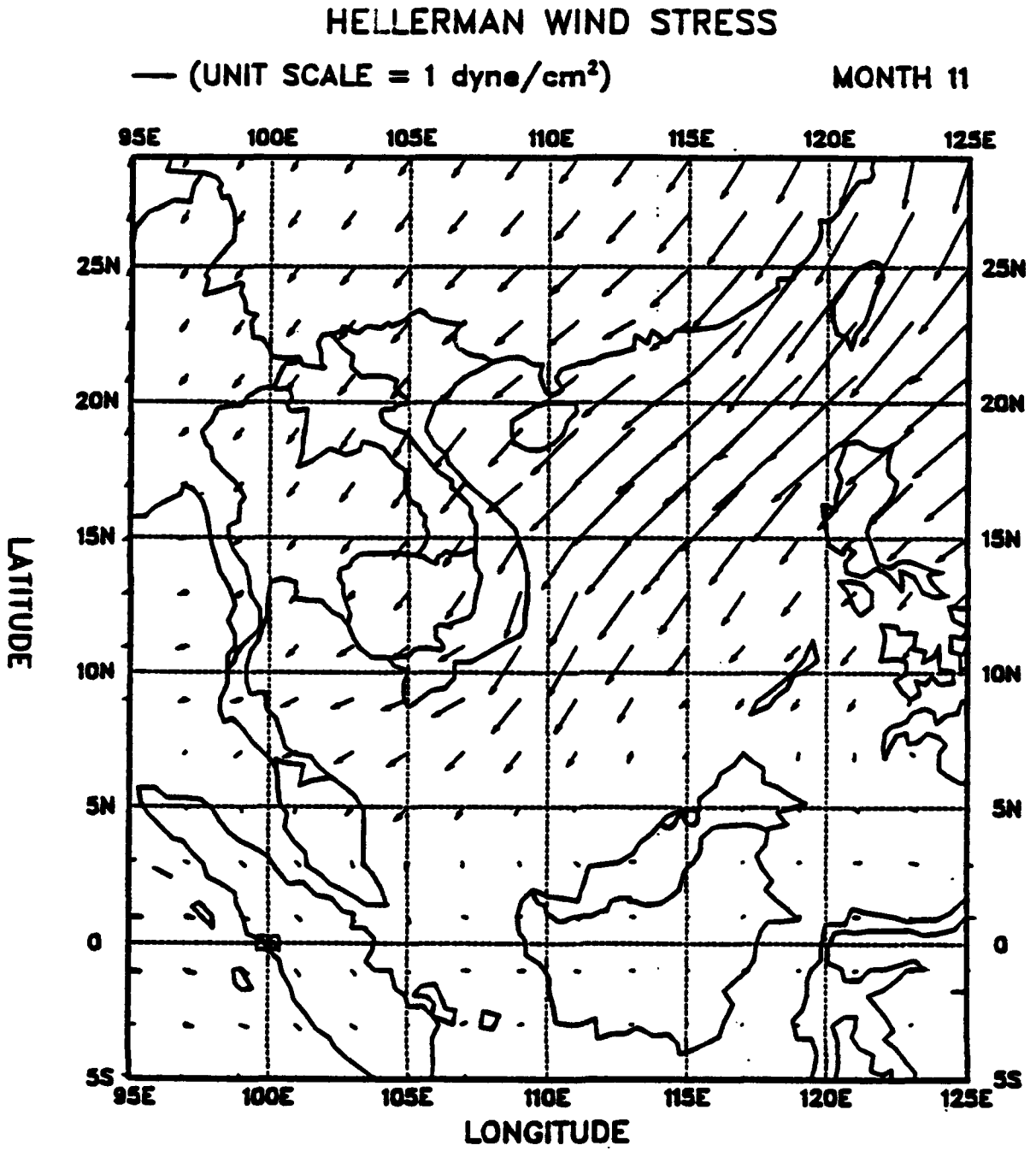

Figure 14C : Winter (November) Hellerman Wind Stress Distribution

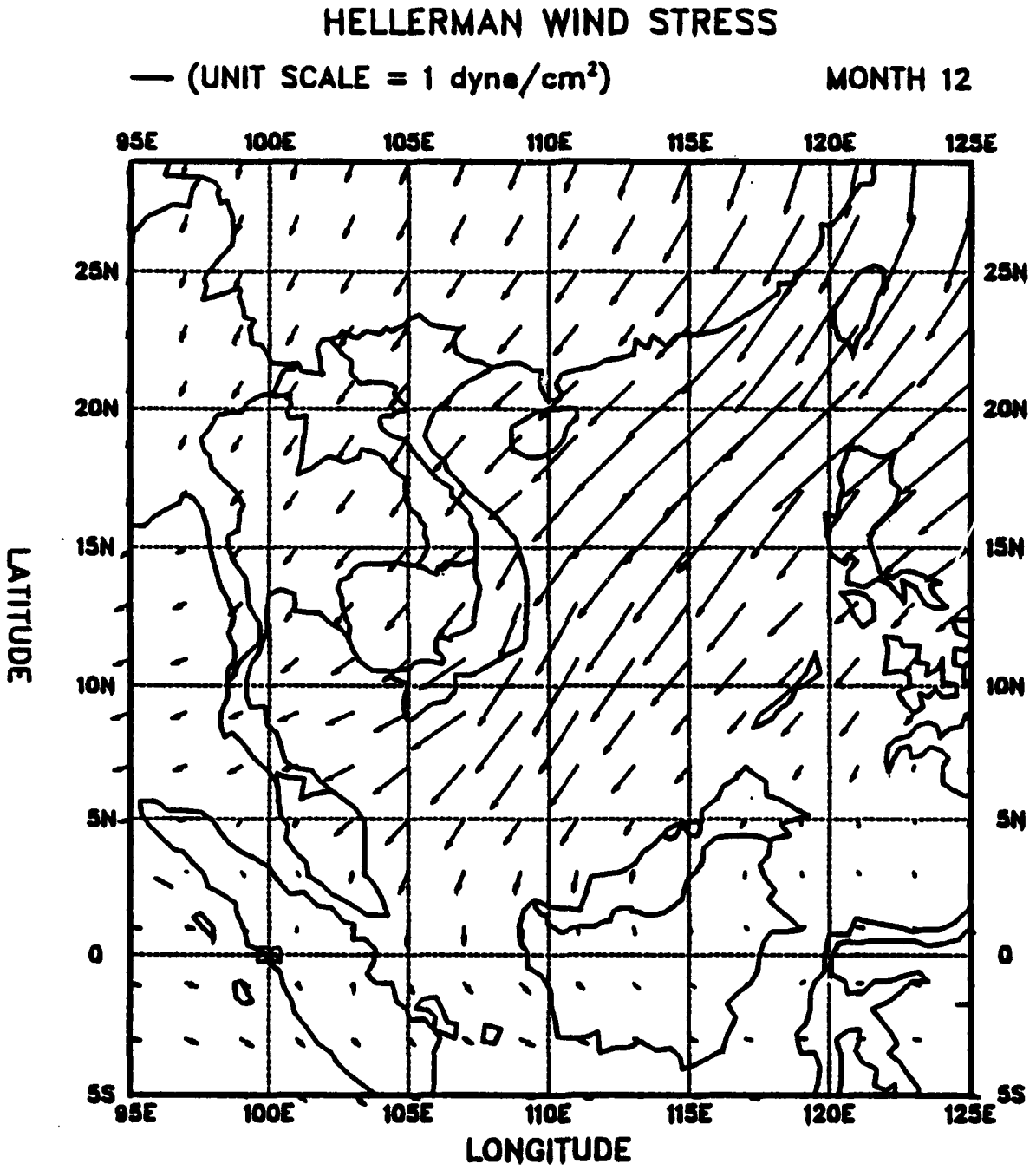

Figure 14D :Winter (December) Hellerman Wind Stress Distribution

IV. MODEL RESULTS

In this study the Princeton South China Sea (PSCS) model is used to simulate the seasonal circulation in the South China Sea. The Naga Report (NR) observations (Wyrtki, 1961) and the Pohlmann shallow-water (PSW) model simulated results (Pohlmann, 1987) are used to compare the performance of the PSCS model in the South China Sea. Because the PSW model provided the simulated summer and winter mean surface circulation patterns and the NR observations provided even-monthly surface circulation depictions, in this study the surface circulation patterns of these two sources are compared to verify the PSCS model results quantitatively. The PSCS model simulated surface temperature and salinity are also discussed to help understand the dynamics of the surface circulation in the South China Sea. Moreover, the comparisons of surface temperature and salinity between the PSCS model and Levitus data (Levitus, 1982) are examined to determine the deviation of the model results from the observations.

The PSCS model started running on 30 April, a time the southwest monsoon is very weak, and was run for one year. The spin-up time of the PSCS model is about 60 days, longer than the 15 days required for the PSW model. The longer spin-up time is due to the fact that the PSCS model's horizontal and vertical resolutions (20 km, 23 levels) are two times higher than the PSW model (50 km, 12 levels).

A. SURFACE CIRCULATION

1. PSCS Model Results

Summer: Because the winter monsoon changes to the summer monsoon in the early part of summer, the time of 10 May may be considered a transition period with monsoon conditions being quite weak (Figure 14A). In response to the weak wind stress on 10 May, the surface current speed is generally quite low over the whole area (Figure 15A). The maximum current speed, about 0.2 m/s, is found in the Gasper and Karimata Straits where waters from the Java Sea enter the South China Sea. On 30 June, summer monsoon prevails (Figure 14B) and surface current speed becomes much faster in the whole region (Figure 15B). Waters from the Java Sea enter the South China Sea through these two straits with a current speed of about 0.7 m/s. Figures 15A and 15B both show that the surface circulation in the Gulf of Thailand is anticyclonic in the summer monsoon season. On 30 June, the waters from the Java Sea divide into two currents between Borneo and Singapore. The largest amount of water flows northward and separates into three branches at about 109°E, 16°N flowing northward along the Vietnam coast, northeastward toward Luzon, and southwestward toward Natuna Island. The northward branch flows into the Formosa Strait. The second branch appears as a strong jet flowing towards Luzon entering the root of the Kuroshio Current through the Luzon Strait. A third branch meets the Borneo Coastal Current at 5°N, 114°E flowing northwards and combines with the jet current from the second branch. The current speed is more than 1 m/s off the coast of Vietnam, about 0.5 m/s off the eastern coast of Hainan, and about 0.2 m/s for the jet current from Vietnam to the Luzon Strait.

Winter: Because the summer monsoon changes to the winter monsoon in late fall, the winter monsoon is weaker on 5 November (Figure 14C) in comparison to the

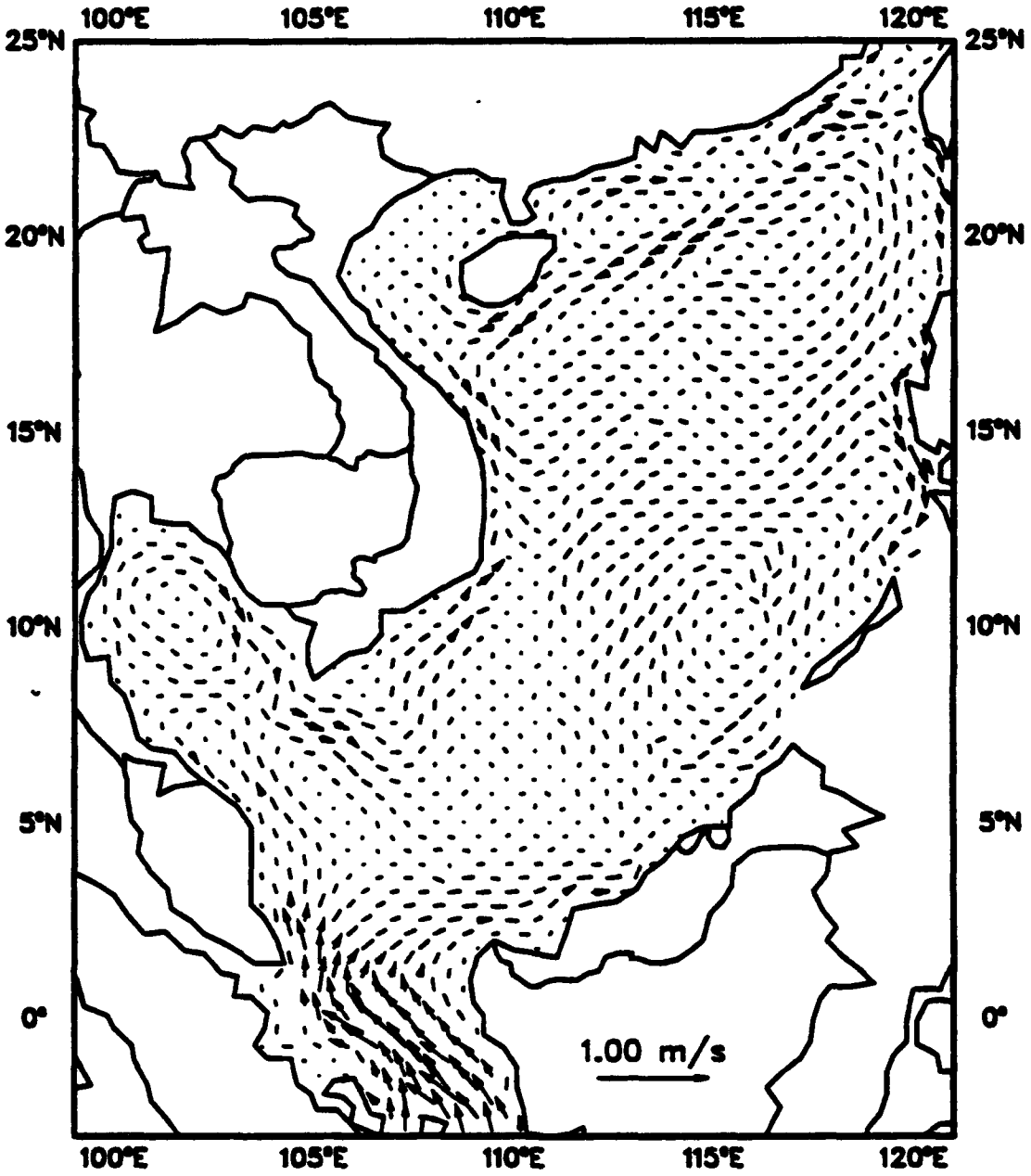

Figure 15A :Simulated Summer (10 May) Surface Circulation

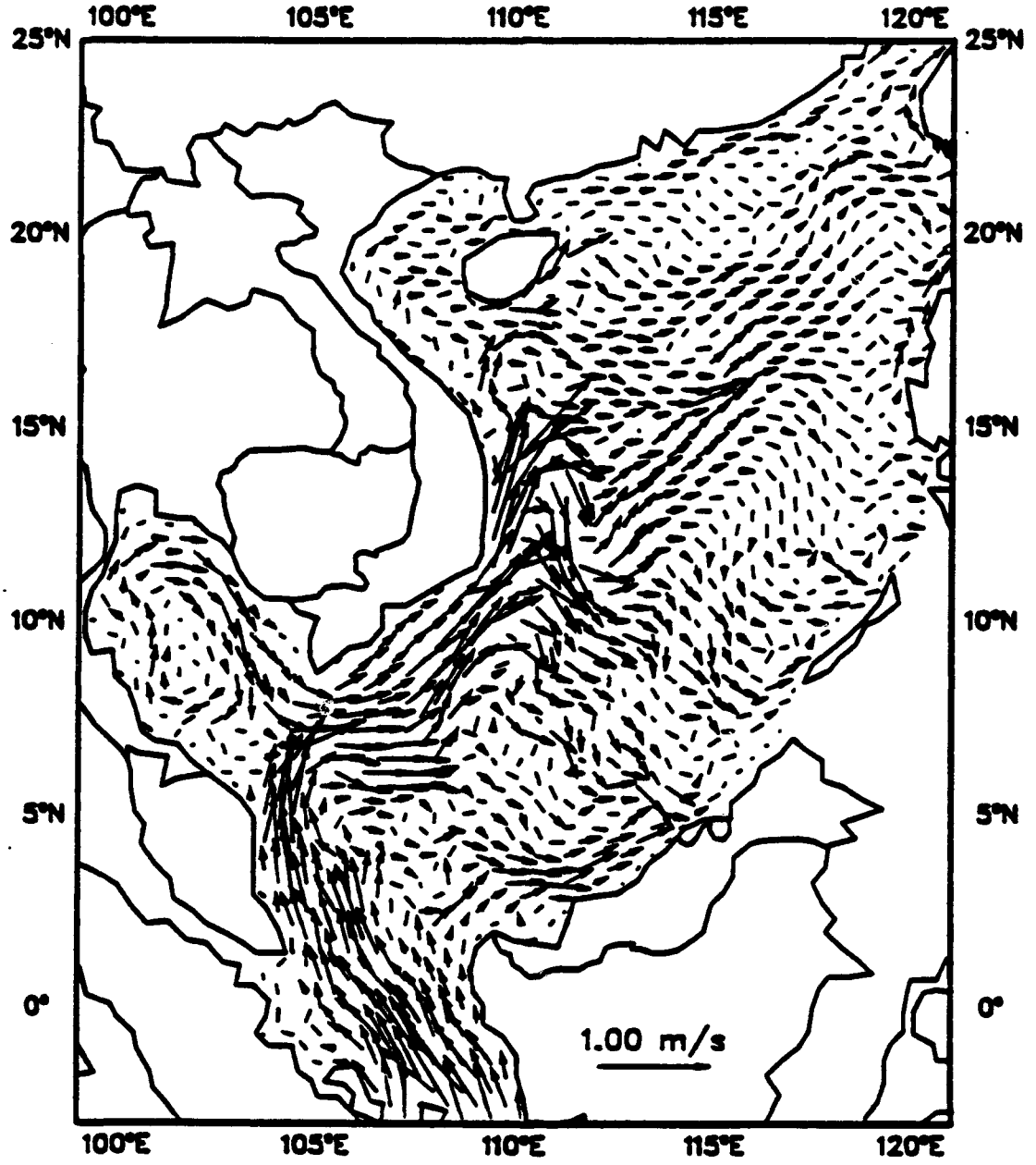

Figure 15B :Simulated Summer (30 June) Surface Circulation

winter monsoon on 10 December (Figure 15D). In response to monsoons on 5 November and 10 December, the surface circulation patterns are similar, but the surface current speed is lower on 5 November (Figure 15C) than on 10 December (Figure 15D). Figures 15C and 15D both show that surface circulation in the Gulf of Thailand is cyclonic in the winter monsoon season. On 10 December, waters from the East China Sea enter the South China Sea through the Formosa Strait. Small branches of water from the Kuroshio Current enter the South China Sea through the Luzon Strait. The water masses from the East China Sea and Kuroshio Current flow southwards along the Chinese and Vietnamese coastlines. This current passes Singapore at about 2°N, 104°E and flows southeastward entering the Java Sea. The waters around Palawan separate into two branches at about 114°E, 10°N. One branch turns right flowing northward and cyclonically along the western coast of Luzon. Then, it turns left at 18°N, 116°E and flows westward towards the coast of China where it joins the main stream of the coastal current flowing southwards along the Hainan and Vietnam coastlines. The second branch flows westward spreading cyclonically around Natuna Island, passing Singapore, and flowing out of the South China Sea through the Karimata and Gasper Straits. The surface current speed is about 0.5 m/s to 0.8 m/s off the eastern coast of Hainan and 0.7 m/s off the coast of Vietnam.

2. Comparisons

The surface circulation pattern comparison among the NR observations, the PSW model, and the PSCS model is investigated to verify the PSCS model and to examine the relative performances of the PSCS and PSW models. Tables 5 and 6 show the comparisons of summer and winter surface circulation patterns among the PSCS model, the PSW model, and the NR observations. Although the PSCS model exhibits some disagreements with the NR observations in the central part of the South China Sea and the region around Palawan

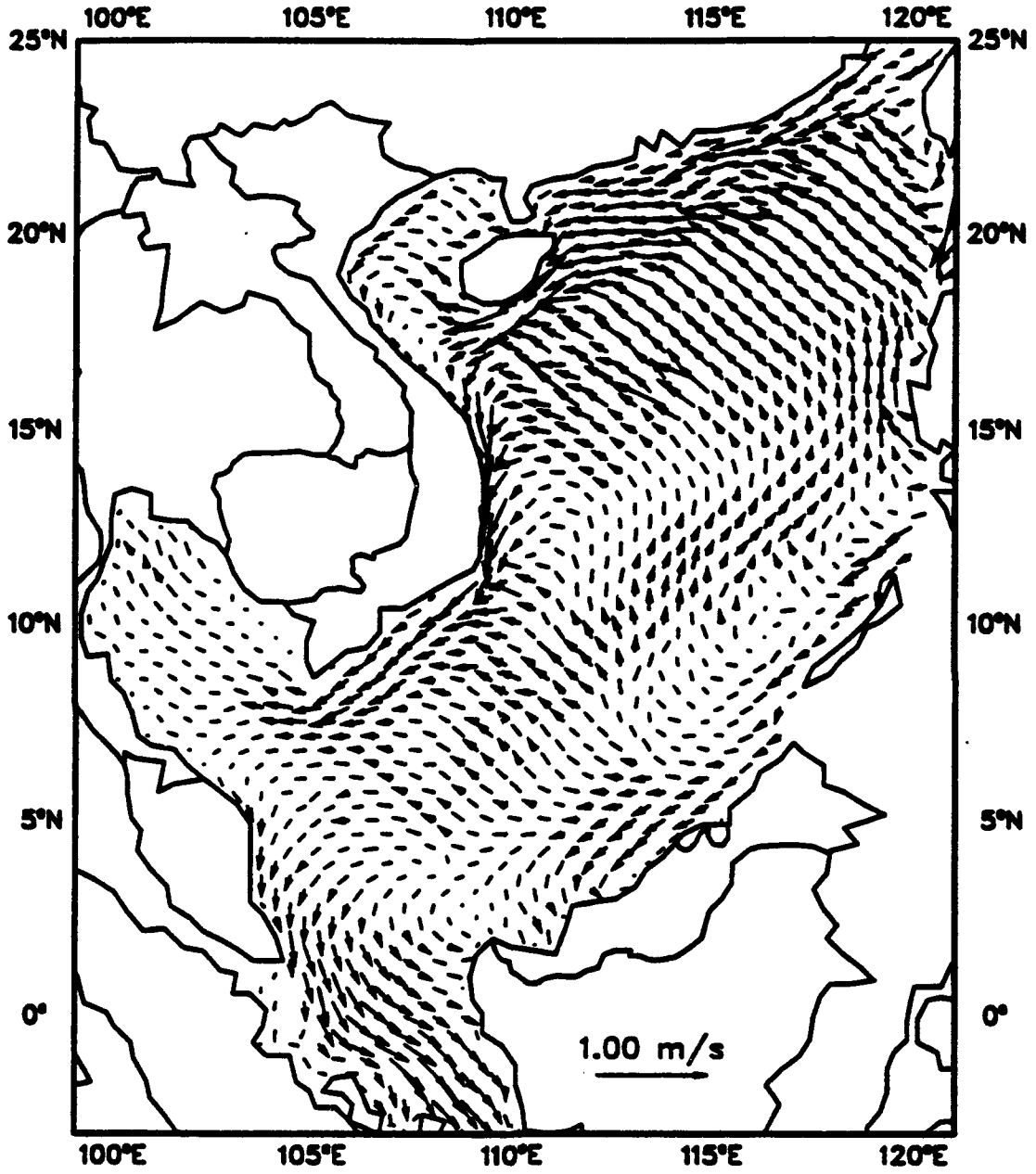

Figure 15C :Simulated Winter (5 November) Surface Circulation

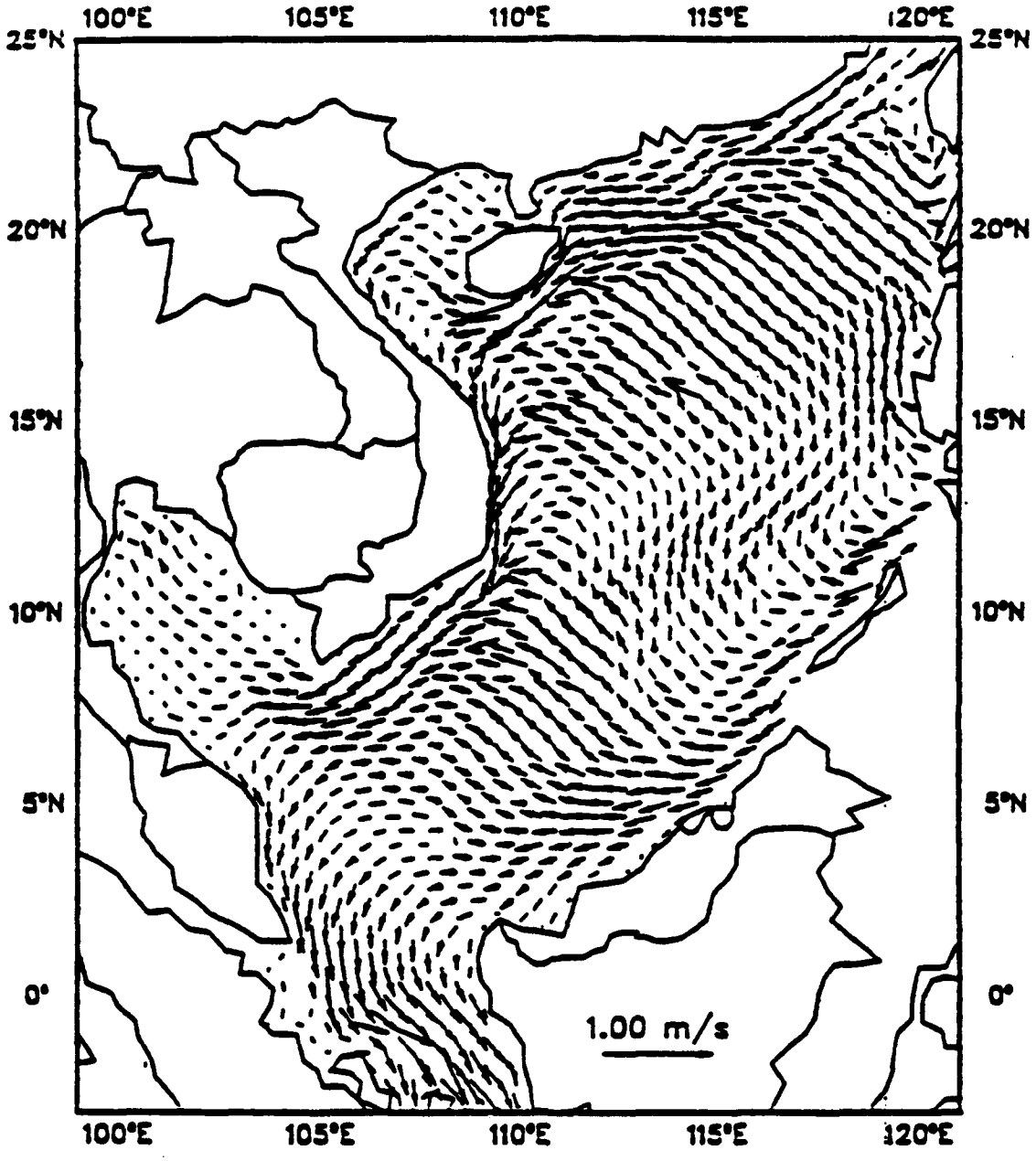

Figure 15D :Simulated Winter (10 December) Surface Circulation

TABLE 5: COMPARISON BETWEEN THE NAGA REPORT AND MODELING RESULTS (SUMMER)

Locations	Naga Report (Wyrtki, 1961) (June)	Shallow-Water Model(Pohlmann) (Summer)	Princeton South China Sea Model (30 June)
Formosa Strait	Out Flow: The south China Sea warm current flows into the Strait.	Out Flow: The South China Sea warm current and the branch of Kuroshio current enter the Strait.	Same as the Naga Report.
Luzon Strait	Out Flow: Currents flow along the western coast of Luzon, cross the southern tip of Taiwan and then enter the Kuroshio main stream.	In Flow: A Kuroshio branch flows into the South China Sea through the northern Luzon Strait. Out Flow: The South China Sea warm current flows out of the South China Sea through the southern Luzon Strait.	Same as the Naga Report
Western Coast of Luzon	Currents flow northwards along the western coast of Luzon.	Currents flow southwards along the western coast of Luzon.	Same as the Naga Report
Coast of Vietnam	(1).Longshore currents flow northeastward. (2). A branch of currents turn backward from off Vietnam to the south. (3). A jet current flow toward the Luzon Strait.	The currents spread all over the central South China Sea and flow to the western coast of Luzon.	Same as the Naga Report.
Region around Palawan	Waters from the Sulu Sea spread into the Dangerous Ground.	Waters from the western side flow towards Palawan.	Waters from the western side flow towards Palawan.
Central South China Sea	Currents flow northeastward from the coast of Vietnam.	Currents flow eastwards from the coast of Vietnam.	Same as the Naga Report.
Karimata Strait	In Flow	Same as the Naga Report.	Same as the Naga Report
Gulf of Tonkin	clockwise circulation	(not clear)	Same as the Naga Report.
Gulf of Thailand	clockwise circulation	Same as the Naga Report	Same as the Naga Report.

TABLE 6: COMPARISION BETWEEN THE NAGA REPORT AND MODELING RESULTS (WINTER)

Locations	Naga Report (Wyrtki, 1961) (December)	Shallow Water Model (Pohlmann) (Winter)	Princeton South China Sea Model (10 December)
Formosa Strait	In Flow: Waters from the East China Sea flow *into* the South China Sea.	Out Flow: A branch of Kuroshio current enters the Strait.	Same as the Naga Report.
Luzon Strait	In Flow: A small branch of Kuroshio current enters the South China Sea	In Flow: Large amount of Kuroshio current flows into the South China Sea.	Same as the Naga Report
Western Coast of Luzon	Current flow northwards along the western coast of Luzon.	Currents flow southwards along the western coast of Luzon.	Same as the Naga Report
Coast of Vietnam	Longshore currents flow southwards.	Same as the Naga Report.	Same as the Naga Report.
Region around Palawan	Waters from the Sulu Sea enter the South China Sea flowing northward.	Waters from the north flow southward along the Palawan coastline.	Same as the Naga Report
Central South China Sea	Currents flow counterclockwise and current boundary exists.	Currents flow westwards from the western coast of Luzon and spread all over the central South China Sea.	Waters flow northwards, turn left to the coast of Hainan and then flow to the coast of Vietnam. Then it enters the main stream go southwards. Unlike the Naga Report the waters continue southward and do not form a current boundary.
Karimata Strait	In Flow	Same as the Naga Report.	Same as the Naga Report
Gulf of Tonkin	counterclockwise circulation	(not clear)	Same as the Naga Report.
Gulf of Thailand	counterclockwise circulation	Waters inflow from the South China Sea	Same as the Naga Report.

(the region between the Dangerous Ground and the Mindoro and Balabac Straits), the overall performance is much better than the PSW model.

Summer: During the summer monsoon season, both models show the surface currents flowing northward in response to the southwest monsoon. The PSW model demonstrated a good performance in the Karimata Strait and the Gulf of Thailand. However, it fails in the Formosa and Luzon Straits, the central South China Sea, the region around Palawan, and the coast of Vietnam. The PSW model results show that the waters from the Kuroshio Current enter the South China Sea through the Luzon Strait, and then flow northward into the Formosa Strait. However, the NR observations show that waters of the Kuroshio Current do not enter the South China Sea in this season. In the central South China Sea, the PSW model results show that currents flow eastward from the coast of Vietnam to the region around Palawan, which are oppositely directed compared with the NR observations. Moreover, off the coast of Vietnam, the PSW model simulated currents do not show jet branching flowing northeastward from the Vietnam coast to the Luzon Strait, which was reported by Wyrtki (1961). However, except for the region around Palawan, the PSCS model results match the NR observations very well. The PSCS model results show that the surface currents flow eastward towards the Palawan in the region around Palawan, which are oppositely directed compared with the NR observations.

Winter: During the winter monsoon season, two models show that the surface currents flowing southward in response to the winter monsoon winds. The PSW model shows good performance along the coast of Vietnam and around the Karimata Strait. It fails in the Formosa and Luzon Straits, the central South China Sea, the region around Palawan, and the Gulf of Thailand. The PSW model results show that a large amount of Kuroshio Current flows into the South China Sea through the Luzon Strait, and then flows out of the South China Sea through the Formosa Strait. However, the NR observations show that a small amount of Kuroshio Current flows into this region through the Luzon Strait, and a large amount of water flows into the South China Sea through the Formosa Strait. In addition, in the central South China Sea, the PSW model results show that currents flow

westward from the western coast of Luzon and spread all over the central South China Sea, but the NR observations show a current boundary exists in the central South China Sea. In the Gulf of Thailand and the region around Palawan, the PSW model simulated surface currents are oppositely directed compared with the NR observations. Except for the central South China Sea, the PSCS model matches the NR observations very well. In the central South China Sea, the PSCS model results do not show the current boundary (which is reported by Wyrtki (1961)).

The comparisons of current speeds between the NR observations and the PSCS model results are made off the coast of Hainan, off the coast of Vietnam, and the Gasper Strait in both summer (Table 7) and winter (Table 8). The comparisons show very good agreements in both summer and winter seasons. In summer, they both show that surface current speed is about 0.5 m/s off the coast of Hainan, more than 1 m/s off the coast of Vietnam, and about 0.7 m/s in the Gasper Strait. In winter, they both show about 0.5 m/s off the coast of Hainan, about 0.7 m/s off the coast of Vietnam, and 0.3 m/s in the Gasper Strait.

TABLE 7: COMPARISON OF CURRENT SPEED BETWEEN THE NR OBSERVATIONS AND THE PSCS MODEL RESULTS (JUNE)

Locations	The NR Observations	The PSCS Model
Off Eastern Coast of Hainan	0.5 m/s	0.5 m/s
Off Coast of Vietnam	> 1.0 m/s	> 1.0 m/s
The Gasper Strait	0.75 m/s	0.7 m/s

TABLE 8: COMPARISON OF CURRENT SPEED BETWEEN THE NR OBSERVATIONS AND THE PSCS MODEL RESULTS (DECEMBER)

Locations	The NR Observations	The PSCS Model
Off Eastern Coast of Hainan	0.5 m/s	0.5m/s - 0.8 m/s
Off Coast of Vietnam	0.75 m/s	0.7 m/s
The Gasper Strait	0.3 m/s	0.35 m/s

The PSCS model improves upon the performance of the PSW model for the simulation in the South China Sea. However, there are some discrepancies between the PSCS model results and the NR observations. The discrepancies occur in the region around Palawan and the central South China Sea during the summer and winter monsoon seasons, respectively. In summer, the NR observations show that water from the Sulu Sea enters the South China Sea spreading into the Dangerous Ground, but the PSCS model results show an eastward water flow toward Palawan. In winter, the NR observations show that a shear zone is present in the central South China Sea, but the PSCS model does not show the same pattern in this area. These might be caused by the complex bottom topography of the Dangerous Ground, the artificially enclosed open boundaries, and the data interpolation.

B. TEMPERATURE AND SALINITY

1. PSCS Model Results

The PSCS model simulated surface temperature and salinity distributions for the summer and winter monsoon seasons are shown in Figures 16 and 17, respectively. We can clearly see that the warm water moves northward during the summer monsoon season and that cool water spreads southward during the winter monsoon season (Figure 16). In response to the change of monsoon-driven surface circulations, the water properties near the open boundaries also show strong seasonal variations. The East China Sea, with cool and high salinity waters, is an adjacent sea which can supply different water masses for the South China Sea. We also observe a seasonal variation of the warm, saline water in Figures 16 and 17, northward advance during summer and southward retreat during winter. The surface salinity in the South China Sea is affected by the water of the adjacent seas which is carried by the currents and surface dilution.

Summer: During the summer monsoon season (June) (Figure 16A), in response to the southwest monsoon (Figure 14A), warm water moves northeastward and there is upwelling of cooler (about 24°C) water along the coastlines of Vietnam and Hainan. Large

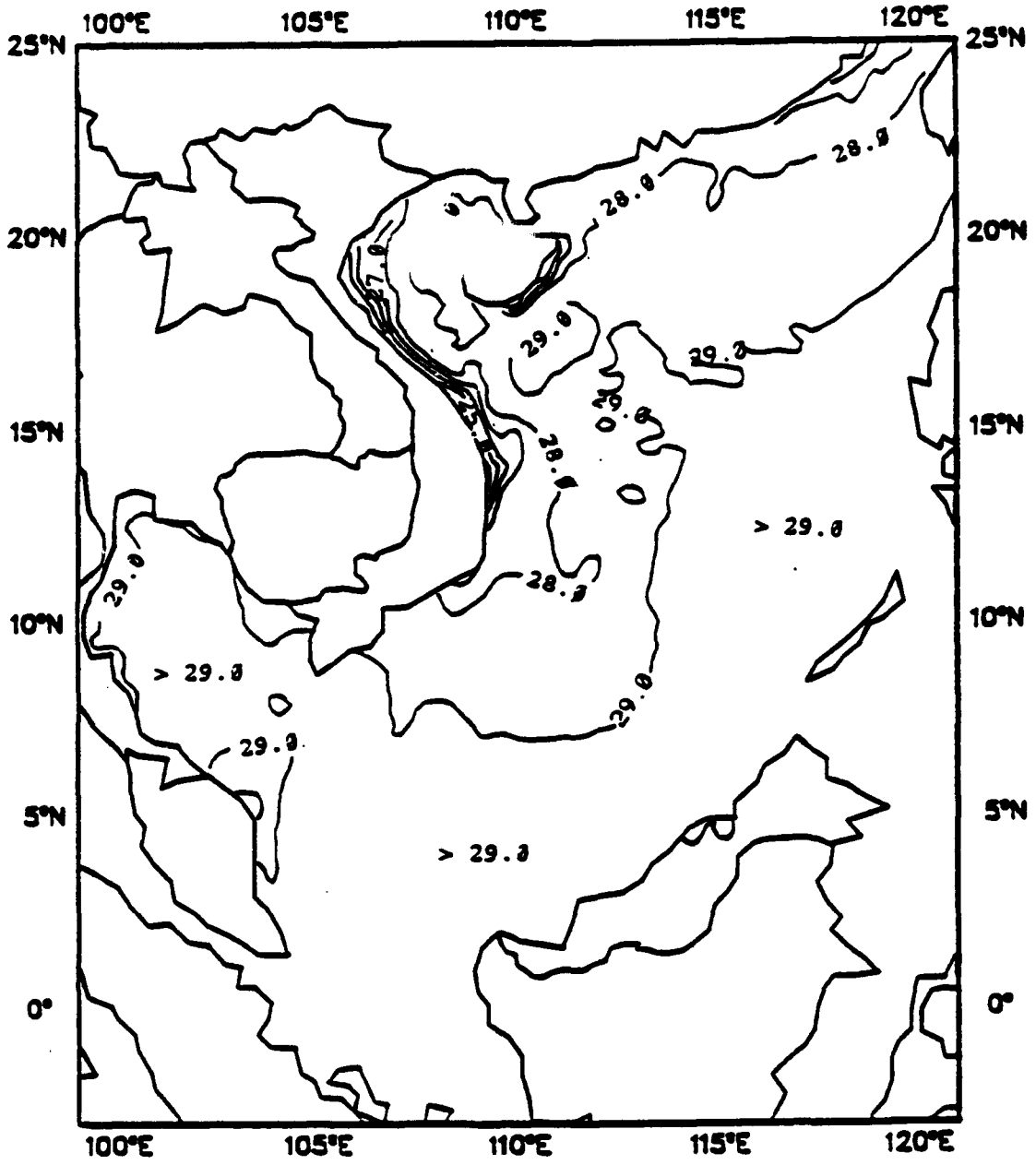

Figure 16A :Simulated Summer (30 June) Surface Temperature (°C)

Distribution; Interval = 1°C

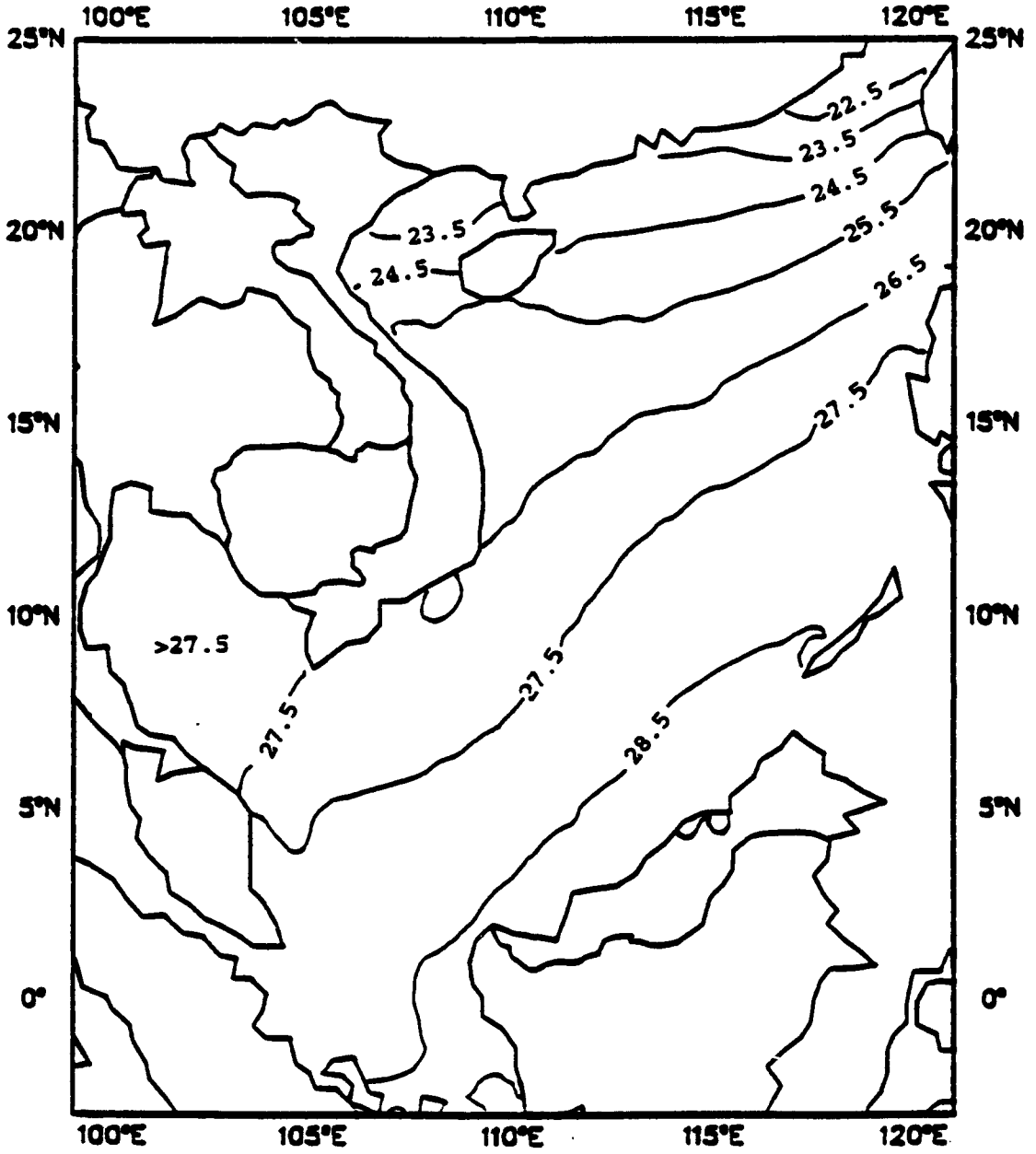

Figure 16B :Simulated Winter (10 December) Surface Temperature (°C)

Distribution; Interval = 1°C

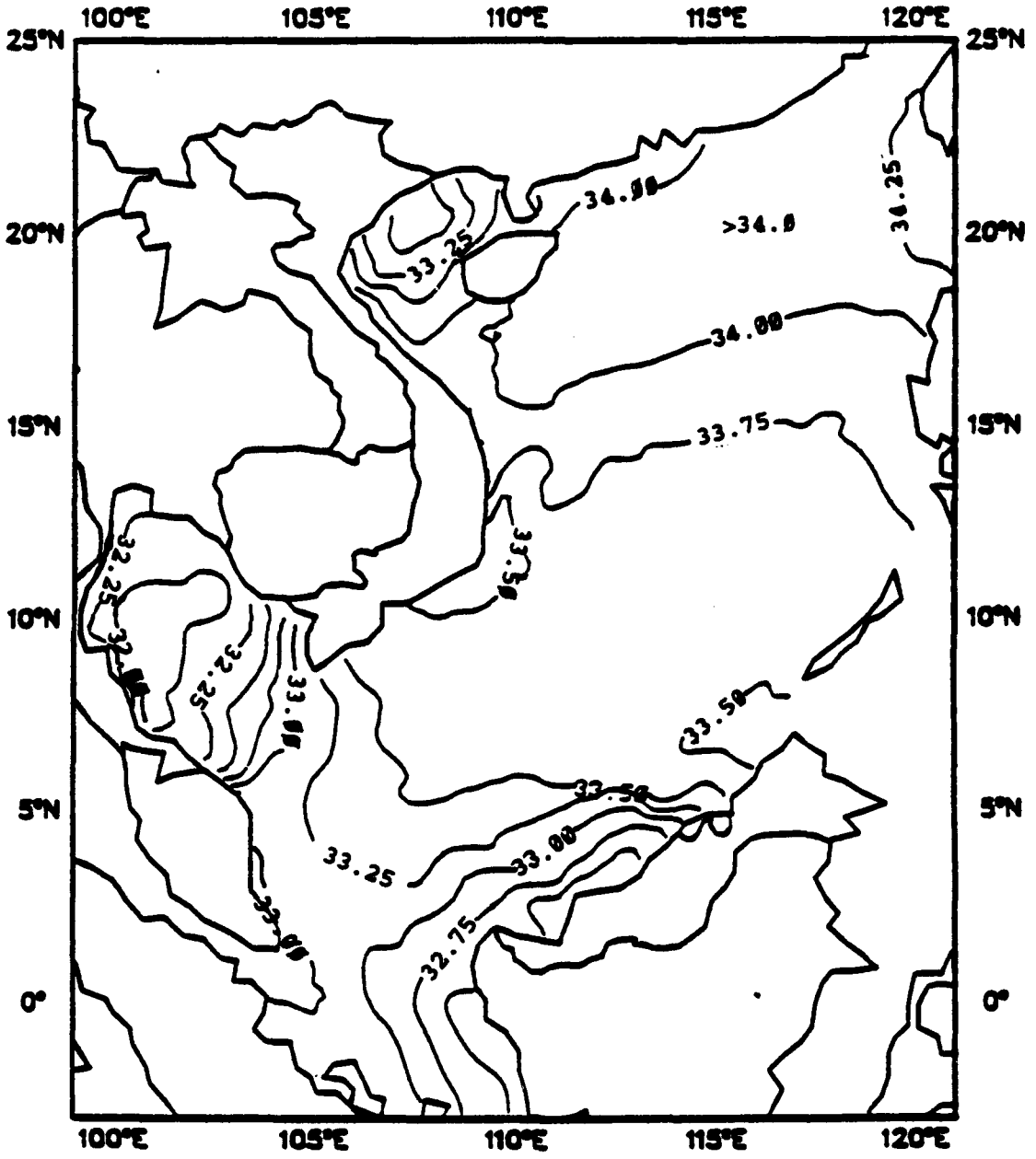

Figure 17A : Simulated Summer (30 June) Surface Salinity (psu) Distribution;

Interval = 0.25 psu

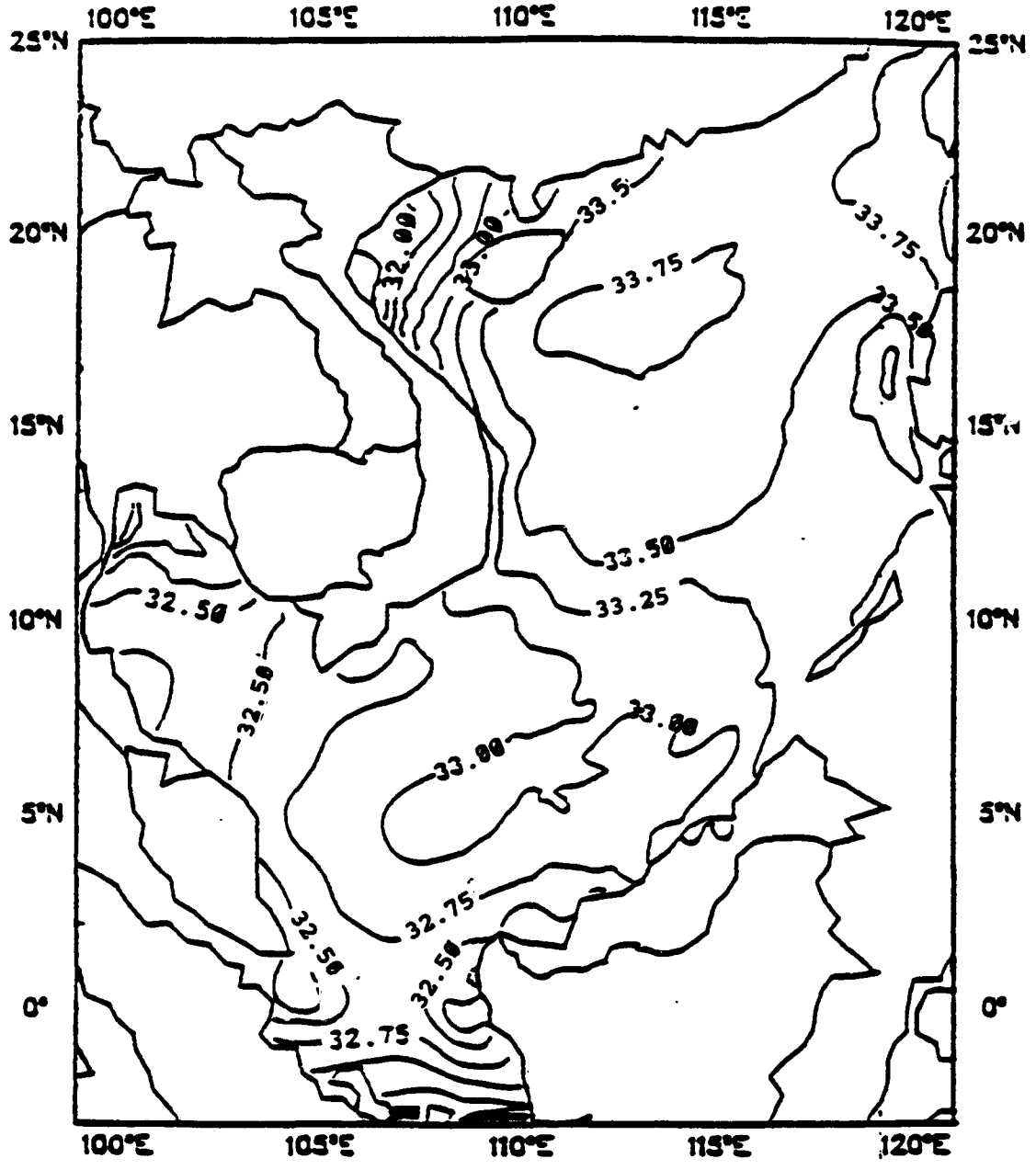

Figure 17B :Simulated Winter (10 December) Surface Salinity (psu) Distribution;

Interval = 0.25 psu

horizontal temperature gradient occur in the upwelling regions. The highest temperatures (about 30°C) occur in the Gulf of Thailand. Other areas of warm water are off the coast of Borneo and the Sunda Shelf. On the other hand, the temperature distributions are homogeneous (~28°C) in most of the northern parts and the other areas of the South China Sea. The surface temperature in the narrow area between the Asian coastline and the 28°C isotherm, including the Formosa Strait, the Gulf of Tonkin, and the shelf off the coast of Vietnam, is between 24°C and 28°C. The southwest monsoon-driven coastal upwelling, with surface temperatures lower than 24°C, occurs in this region.

During the summer season, the surface salinity increases northeastward from 32.75 psu off the Borneo coast to 34.25 psu on the western side of the Luzon Strait (Figure 17A). Large salinity gradients occur at the coast of Borneo, the Gulf of Thailand, and the Gulf of Tonkin. In response to the southwest monsoon, water masses from the Java Sea enter the Sunda Shelf and flow northward along both the western and eastern sides of the South China Sea. Because of the surface river runoff into the Gulf of Thailand and around Borneo, the surface salinity in the Gulf of Thailand is about 32.0 psu to 33.0 psu, and is about 32.5 psu to 33.0 psu around Borneo. Because of river runoff, less saline water is found off the southern coast of Vietnam (surface salinity is less than 33.0 psu), and off the Gulf of Tonkin (surface salinity between 33.0 psu and 33.75 psu). In the northern South China Sea, because it connects with the cooler and more saline waters from the north, the surface salinity is greater than 34.0 psu. In the central South China Sea, surface salinity is very homogeneous, about 33.5 psu to 34.0 psu.

Winter: During the winter monsoon season (December) (Figure 16B), in response to the northeast monsoon winds (Figure 14D), cool waters flow southwestward from the East China Sea entering the northern South China Sea through the Formosa Strait. The isotherms are aligned northeast-southwest increasing from the Formosa Strait to Singapore. Coastal upwelling disappears in this season. Because of the different water masses mixing strongly, the largest temperature gradients occur in the vicinity of Formosa

Strait with the temperature ranging from 21.5 and 22.5°C. In the Gulf of Tonkin, surface temperatures range between 23.0 and 25.5°C. In the Gulf of Thailand surface temperatures are higher than 27.5°C. Maximum temperatures of 28.5°C are found off the coast of Borneo.

During the winter season, surface salinities increase from 32.50 psu in the south to 33.75 psu in the north (Figure 17B). The cooler high salinity waters from the East China Sea flow with the southwestward currents entering the northern South China Sea. The surface salinity in the northern South China Sea is between 33.5 psu and 34.0 psu which is higher than the other regions of the South China Sea. Because of the river runoff, the largest salinity gradients occur in the Gulf of Tonkin, the Gulf of Thailand and the constriction between Sumatra and Borneo. In the Gulf of Tonkin the surface salinity ranges from 31.75 psu to 33.25 psu. On the other hand, in the Gulf of Thailand, the surface salinity ranges from 31.5 psu to 32.75 psu. In the southern and central South China Sea, surface salinities are homogeneous between 32.5 psu and 33.5 psu. Between the Sumatra and Borneo, the surface salinity gradient is larger than the other places, and it ranges from 32.75 psu to 33.75 psu.

2. Comparisons

The PSCS model results show good agreement with the Levitus temperature and salinity data. The comparison between PSCS model results and Levitus data is described as follows.

a. Temperature

The PSCS model simulated surface temperature (Figure 16) matches the Levitus temperature data (Figure 11) very well. During summer (June), the PSCS model results show that there is cool water off the coast of Vietnam and the southwest monsoon -induced upwelling occurs along the coastline of Vietnam and Hainan. The Levitus data does not show strong coastal upwelling, but it does show that cool water occurs off the coast of Vietnam. However, according to Wyrtki (1961), wind-driven upwelling is found along the

coastlines of Vietnam and Hainan in the southwest monsoon season. During winter (December), both the PSCS model results and the Levitus data show that the cold waters move southwestward.

b. Salinity

The PSCS model simulated surface salinity (Figure 17) matches the Levitus salinity data (Figure 12) reasonably well in most parts of the South China Sea, except at the coastal region of the Gulf of Thailand, the Gulf of Tonkin, and around Borneo where the PSCS model simulated surface salinity is generally greater than the Levitus salinity data regardless of seasons. For example, at the coastal region of the Gulf of Thailand, the PSCS model results show that surface salinities are about 32.25 psu in summer, and 31.5 psu in winter, respectively. In the same region the Levitus salinity data show that surface salinities are about 32.25 psu in summer, and 30.75 psu in winter, respectively. This could be caused by the exclusion of some physical processes in the PSCS model, such as the heavy river runoff.

V. CONCLUSIONS

The Princeton South China Sea (PSCS) model was used to investigate the seasonal surface circulation in the South China Sea. An analysis of the simulated surface circulation shows that the South China Sea exhibits a strong seasonal variation for surface circulation in response to the seasonal monsoons. Also, surface temperature and surface salinity which are studied in this simulation show that most of the surface ocean dynamics of the South China Sea are strongly affected by the monsoons.

During the summer monsoon season, southwest winds prevail and the main surface current flows westward from the Java Sea through the Karimata and Gasper Straits, then flows northeastward from Singapore along the coast of Asia toward the Luzon and Formosa Straits. The jet current from Vietnam to Luzon is very evident in this season. The current is stronger in the southern South China Sea and the current speed is about 0.5 m/s off the eastern coast of Hainan, more than 1 m/s off the coast of Vietnam, and about 0.75 m/s between Singapore and Borneo, respectively. Upwelling with a temperature of 24.0°C is induced and found off the coastlines of Vietnam and Hainan. Warm waters flow northward (warm advection) during this season. The surface temperature is between 28°C and 29°C in the South China Sea. The surface salinity is between 33.5 psu and 34.25 psu in the northern and central South China Sea, between 32.0 psu and 33.0 psu in the Gulf of Thailand, and between 32.5 psu and 33.0 psu near the coast of Borneo.

During the winter monsoon season, northeast winds prevail and upwelling disappears. The main surface current flows southwestward from the Luzon and Formosa Straits along

the coast of Asia toward Singapore, then flows eastward through the Karimata and Gasper Straits entering the Java Sea. This coastal current dominates most of the South China Sea. Another current which flows from Borneo to Vietnam is also important during this season. The current speed is about 0.8 m/s off the eastern coast of Hainan and 0.7 m/s off the coast of Vietnam. The surface temperature is about 27.5°C in the southern South China Sea and is between 24.5°C and 27.5°C in the northern South China Sea. The surface salinity is between 33.0 psu and 34.0 psu in the northern and central South China Sea, between 31.5 psu and 32.75 psu in the Gulf of Thailand, and between 32.25 psu and 32.75 psu near the coast of Borneo.

The PSCS model simulated temperature field is much closer to the observational data than the salinity field, especially in the coastal regions. This is due to the exclusion of the river runoff process in the PSCS model. Most of the PSCS model-generated results of this study match the NR observations quite well and provide more detailed information than the PSW model. However, some model discrepancies with the NR observations still exist, especially the winter surface currents in the central part of the South China Sea, and the summer surface currents near Palawan. The discrepancies may be caused by artificially enclosing the four open boundaries (the Strait of Malacca, Banka Strait, Mindoro Strait, and Balabac Strait) or by the interpolation of sparse data sets.

Four recommendations are provided for future studies. First, a high resolution database should be established including the atmospheric and the oceanic features. In this way, errors due to the interpolation of sparse data sets can be reduced. Second, use realistic open boundary conditions. Third, the model physics needs to be improved (e.g., including river runoff). Fourth, better measurements of the bathymetry near the Dangerous Ground

should be made. The discrepancies between this simulation and the observations in the central part of the South China Sea and the region around the Palawan (which is the region between the Dangerous Ground and the Mindoro and Balabac Straits), may have been caused by the poor bottom topographical data of the Dangerous Ground.

LIST OF REFERENCES

1. Broecker, W. S., W. C. Patzert, and M. Stuiver, 1986, Hydrography, chemistry, and radiotopes in the Southeast Asian basins, J. Geophys. Res., Vol. 91, No. C12, 14345-14354.

2. Blumberg, A. F., and G. L. Mellor, 1987, A description of a three-dimensional coastal ocean circulation model, Three-Dimensional Coastal Ocean Models, American Geophysical Union, Washington, D.C., 1-16.

3. Cheang,B.-K., 1987, Short and Long Range Monsoon Prediction in Southeast Asia Monsoons, A Wiley-Interscience Publication, 579-606.

4. Fan, K.-L., 1982, A study of water masses in Taiwan Strait, ACTA Oeanographica Taiwanica, Dec., 140-153.

5. Gilg, J. G., 1970, Bathymetry of the South China Sea, Kuroshio, East-West Center Press, University of Hawaii, 21-28.

6. Hellerman, S. and M. Rosenstein, 1983, Normal monthly wind stress over the world ocean with error estimates, J. Phys. Oceanogr., Vol.13, 1093-1104.

7. Hess, S. L., 1983, Introduction to Theoretical Meteorology, Robert E. Krieger Publishing Co., 328-329.

8. Huang, Y.-X., 1988, Temperature and salinity distributions in the South China Sea and adjacent waters, Prog. Oceanogr., Vol.21, 493-501.

9. Levitus, S., 1982, Climatological atlas of the world ocean, NOAA Professional Paper#13, U.S. Government Printing Office, Washington, D.C.

10. Liahude, A. G., 1979, On the hydrology of the Natuna Sea, Kuroshio IV, Proceedings of the Fourth CSK Symposium, Tokyo, 332-352.

11. Liu, X.-B., J.-L. Su, 1992, A reduced gravity model of the circulation in the South China Sea, Oceano.-Limnol. Vol.23, No.4, pp. 328-336.

12. Mellor, G. L. and T. Yamada, 1982, Development of a turbulence closure model for geophysical fluid problem, Rev. Geophys. Spa. Phys., Vol.20, No.4, 851-875.

13. Neelasri, C. A., 1979, Diagnostic model of the flow in the Gulf of Thailand, Kuroshio IV, Proceedings of the Fourth CSK Symposium, Tokyo, 912-929.

14. Nitani, H., 1970, Oceanographic conditions in the sea east of the Philippines and Luzon Strait in summer of 1965 and 1966, Kuroshio, East-West Center Press, University of Hawaii, 214-232.

15. Pickard, G. L. and W. J. Emery, 1990, Descriptive Oceanography, 5th ed., Pergamon Press, NY, 235-236.

16. Pohlmann, T., 1987, A three-dimensional circulation model of the South China Sea, Three-Dimensional Models of Marine and Estuarine Dynamics, Elsevier Science Publishing Co., Inc., 245-268.

17. Shaw, P.-T., 1989, The Intrusion of water masses into the sea southwest of Taiwan, J. Geophys. Res. Vol. 94, No. C12, 18213-18226.

18. _____ , 1991, The seasonal variation of the intrusion of the Philippine Sea water into the South China Sea, J. Geophys. Res., Vol.96, No.C1, 821-827.

19. _____ , 1992, Shelf circulation off the southeast coast of China, Review. Aquat. Sci., Vol.6, No.1, 1-28.

20. Wyrtki, K., 1961, Scientific Results of Marine Investigations of the South China Sea and the Gulf of Thailand 1959-1961, Naga Report, Vol. 2&3, The University of California Scripps Institution of Oceanography, 1961.

21. Zhong, H.-L., 1990, On relationship between warm current and Kuroshio branch in South China Sea, Mar-Sci-Bull-Haiyang-Tongbao, Vol.9, No.4, 9-15.

INITIAL DISTRIBUTION LIST

		No. of Copies
1.	Defense Technical Information Center Cameron Station Alexandria, VA 22304-6145	2
2.	Dudley Knox Library, Code 52 Naval Postgraduate School Monterey, CA 93943-5002	2
3.	Department Chairman, Code OC Department of Oceanography Naval Postgraduate School Monterey, CA 93943	1
4.	Prof. P. C. Chu, Code OC/CU Department of Oceanography Naval Postgraduate School Monterey, CA 93943	5
5.	Dr. Dong-Shan Ko Department of Applied Marine Physics RSMAS, University of Miami Miami, FL 33143	5